A Journal of the Gesellschaft Deutscher Chemiker

Angewandte International Edition GDCh Chemie

www.angewandte.org

Accepted Article

Title: Caught in Action: Visualizing Dynamic Nanostructures Within Supramolecular Systems Chemistry

Authors: Akhil Venugopal, Lorena Ruiz-Perez, K. Swamynathan, Chidambar Kulkarni, Annalisa Calo, and Mohit Kumar

To be cited as: *Angew. Chem. Int. Ed.* **2022**, e202208681

Link to VoR: https://doi.org/10.1002/anie.202208681

WILEY-VCH

10.1002/anie.202208681

WILEY-VCH

REVIEW

Caught in Action: Visualizing Dynamic Nanostructures within Supramolecular Systems Chemistry

Akhil Venugopal[a], Lorena Ruiz-Perez[a], K. Swamynathan[b, c], Chidambar Kulkarni*[d], Annalisa Calò*[a, e], and Mohit Kumar*[a, f]

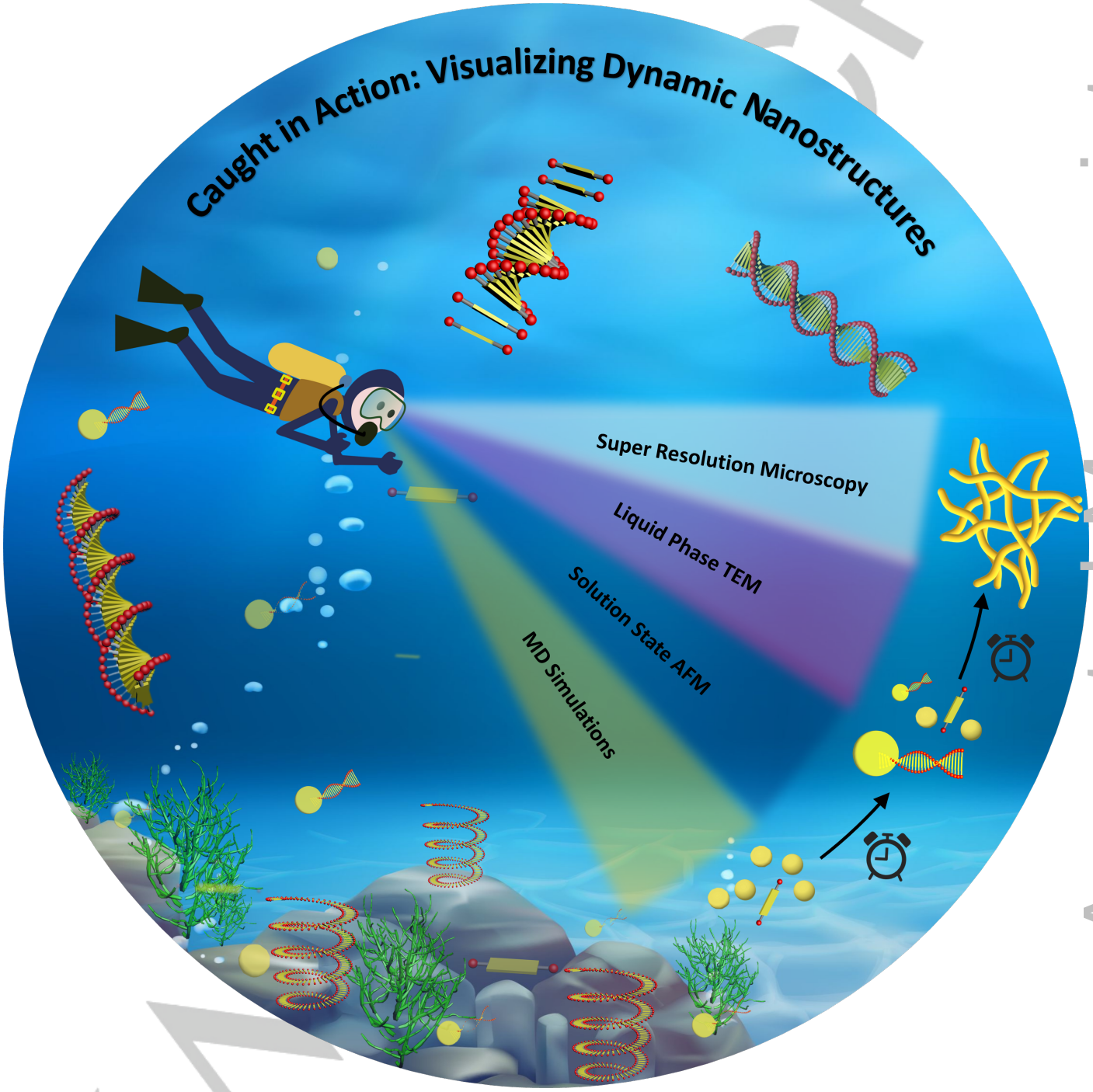

10.1002/anie.202208681

WILEY-VCH

REVIEW

[a] Akhil Venugopal, Dr. Lorena Ruiz-Perez, Dr. Annalisa Calò, and Dr. Mohit Kumar
Institute for Bioengineering of Catalonia (IBEC),
Calle Baldiri Reixac 10-12, Barcelona-08028, Spain
E-mail: mkumar@ibecbarcelona.eu, annalisa.calo@ub.edu
[b] Dr. K. Swamynathan
Soft Condensed Matter, Raman Research Institute
C. V. Raman Avenue, Sadashivanagar, Bangalore-560080, India
[c] Department of Chemistry
NITTE Meenakshi Institute of Technology
Yelahanka, Bengaluru 560064, India
[d] Dr. Chidambar Kulkarni
Department of Chemistry,
Indian Institute of Technology Bombay, Powai, Mumbai-400076, India
E-mail: chidambark@chem.iitb.ac.in.
[e] Department of Electronic and Biomedical Engineering
University of Barcelona, Calle Marti i Fraquès 1-11, Barcelona-08028, Spain
[f] Department of Organic Chemistry
University of Barcelona, Calle Marti i Fraquès 1-11, Barcelona-08028, Spain

Abstract: Supramolecular systems chemistry has been an area of active research to develop nanomaterials with life-like functions. Progress in systems chemistry relies on our ability to probe the nanostructure formation in solution. Often visualizing the dynamics of nanostructures which transform over time is a formidable challenge. This necessitates a paradigm shift from dry sample imaging towards solution-based techniques. We review the application of state-of-the-art techniques for real-time, *in situ* visualization of dynamic self-assembly processes. We present how solution-based techniques namely optical super-resolution microscopy, solution-state atomic force microscopy, liquid-phase transmission electron microscopy, molecular dynamics simulations and other emerging techniques are revolutionizing our understanding of active and adaptive nanomaterials with life-like functions. This Review provides the visualization toolbox and futuristic vision to tap the potential of dynamic nanomaterials.

1. Introduction

Spontaneous organization of molecules in solution results from various non-covalent interactions among molecules to minimize their free energy. This mechanism has been the guiding principle of supramolecular chemistry to form self-assembled nanostructures that are usually at thermodynamic equilibrium and are stable over time. Supramolecular chemistry has been at the forefront of developing functional nanomaterials for applications in the field of organic electronics, nanomedicine, cosmetics,

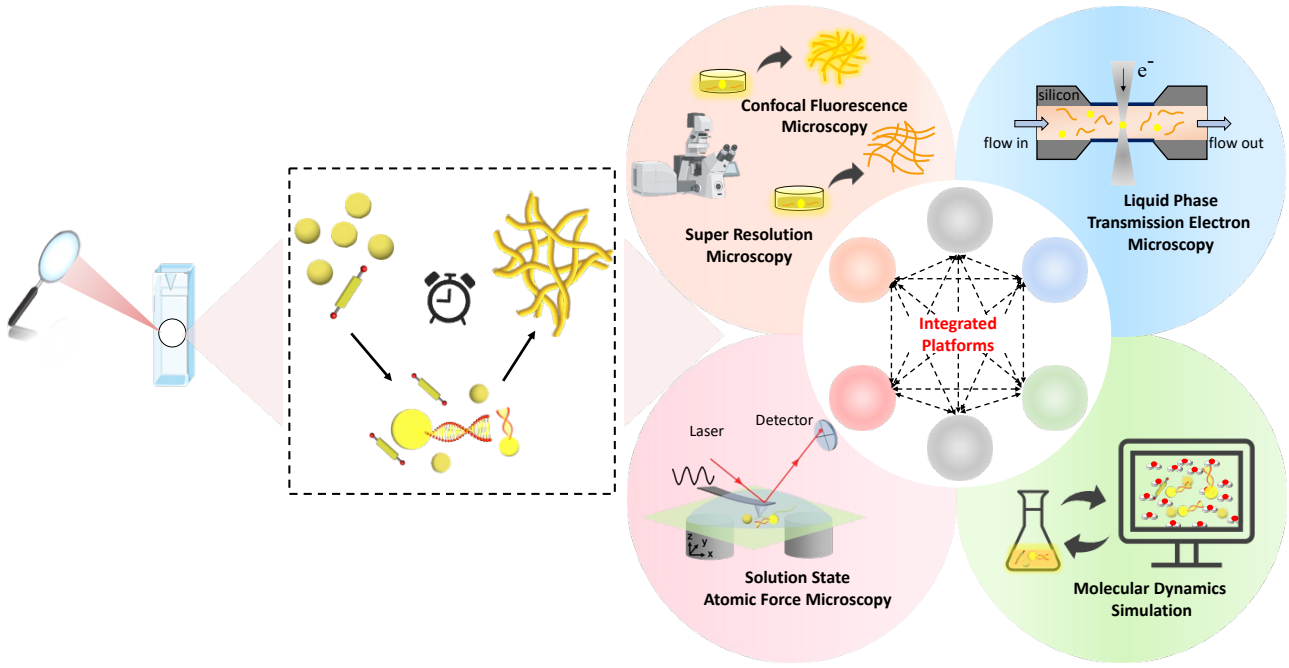

Figure 1. Cartoon representation of dynamic self-assembly processes and the available techniques to visualize such processes in solution, in real-time, *in situ*. The inner white circle depicts a futuristic design where multiple techniques are integrated into a single characterization platform.

sensing and diagnostics among others.[1] Development of novel self-assembled materials relied significantly on our ability to visualize the underlying nanostructures in order to gain complete understanding of the existing material and to design new ones. Since most nanostructures were at equilibrium, they could be visualized by imaging their air-dried samples using atomic force microscopy (AFM), transmission electron microscopy (TEM), cryogenically preserved samples with cryo-TEM, etc. These imaging techniques have provided exceptional details about the supramolecular organization over micro and nanometer down to molecular and atomic length scales, albeit of dry samples which are structurally and functionally static.

In contrast to most synthetic self-assembled systems, the assembly of molecules in living systems are uniquely different. Living structures are highly dynamic and are formed through complex chemical reaction networks to provide kinetic control over structure and function. Biological systems require chemical energy to drive processes out-of-equilibrium, resulting in self-assembled structures which dynamically form and disintegrate over time. Inspired by the dynamic behavior displayed in nature, supramolecular systems chemistry aims to move from equilibrium based stable systems i.e., systems that do not change with time, to dynamic and out-of-equilibrium self-assembly with the aim to obtain life-like functions. Over the past decade, research in such bio-inspired systems has substantially grown. This research effort has resulted in the development of self-assembled nanomaterials with spatial and temporal control over nanostructures, chemical fuel regulated assembly, non-equilibrium catalyst, active droplets etc.[2] Thus, unlike typical self-assembly systems where the investigation of the end point equilibrium nanostructures is often sufficient, dynamic supramolecular systems demands the visualization of time dependent reconfiguration of self-assembly over time.

The advancement of research in dynamic self-assembly has been closely followed by the development of novel microscopic techniques, which can image supramolecular transformation in real-time and *in situ*. These techniques include fluorescence based super-resolution microscopy, AFM and TEM performed in liquid, which have transformed the landscape of imaging supramolecular nanostructures. They are used for solution-state imaging of materials with nanoscale spatial resolution. They can record real-time videos of dynamic transformation to provide an in-depth understanding of the self-assembly processes. Furthermore, *in silico* experiments, performed using Molecular Dynamics (MD) simulations and other computational chemistry techniques, have provided an alternative and sometimes complementary methods to probe dynamic nanostructures, even at times when other methods fail to deliver.

This Review aims to highlight how the research within supramolecular systems chemistry is propelled by the cutting-edge nanostructure visualization techniques. Therefore, only those examples of supramolecular systems which have probed dynamic self-assembling processes will be discussed. There are excellent reviews reported on various examples of supramolecular systems chemistry and their characterization methods, and we direct the readers to get an overview of the field.[3] However, highlighting the examples which demonstrate real-time visualization of dynamic self-assembly process and how it provides crucial information about the nanostructure is a completely new endeavor. The present Review intends to act as a guide to better understand the existing systems as well as provide a toolbox for the design and characterization of future dynamic nanomaterials. This Review is divided into five parts based on the type of visualization techniques introduced: i) fluorescence based super-resolution microscopy; ii) solution state AFM (SS-AFM); iii) liquid phase TEM (LP-TEM); iv) MD simulations; iv) emerging techniques (Figure 1). Finally, we will summarize by providing a critical analysis of the current techniques, their possibilities, and limitations. We will conclude by assessing the current state of the art to contextualize the vision for the future in supramolecular systems chemistry and the role of visualization techniques in the advancement of the field.

Akhil Venugopal is currently pursuing his PhD at Institute for Bioengineering of Catalonia, IBEC under the supervision of Dr Mohit Kumar and Prof. Giuseppe Battaglia. He completed his Integrated BS-MS degree from the Indian Institute of Science Education and Research (IISER), Mohali, India. His research interest is to develop adaptive materials for targeted drug delivery.

Lorena Ruiz-Perez is an imaging scientist and deputy lead of the Molecular Bionics Lab at the Institute for Bioengineering of Catalonia, IBEC in Barcelona Spain. She has expertise in *in situ* transmission electron microscopy imaging of soft organic and biological systems in liquid phase, and focusses on establishing novel techniques for structure reconstruction, image analysis and experimental settings. Lorena holds a master's degree in Physics from the University of Seville and a Ph.D. in Polymer Physics from the University of Sheffield in UK.

K. Swamynathan completed his B.Sc. and M.Sc. in Chemistry from Sri Sathya Sai University, India in 2007 and 2009 respectively. He completed Ph.D. from Raman Research Institute, India under the guidance of Prof. Sandeep Kumar in 2020. He is currently working as Assistant Professor in the Department Of Chemistry, NITTE Meenakshi Institute of Technology, Bengaluru. His research focuses on design, synthesis and characterization of liquid crystalline materials.

Chidambar Kulkarni obtained his MS and Ph.D. degree in 2011 and 2015, respectively from Jawaharlal Nehru Centre for Advanced Scientific Research, India. From 2015 he worked as a Marie-Skłodowska-Curie postdoctoral fellow with Prof. E. W. Meijer at Eindhoven University of Technology, the Netherlands. Since 2020 he is an Assistant Professor in the department of chemistry at Indian Institute of Technology Bombay, India. His main research interests include understanding self assembled systems and chiral materials using experimental and computational tools of Physical-Organic Chemistry.

Annalisa Calò is an Assistant Professor at the University of Barcelona. She holds a Master's degree in Materials Chemistry and a PhD in Chemical Sciences from the University of Bologna. She has been postdoctoral fellow in different institutions in Spain (IBEC, ICN2 and CIC nanoGUNE) and in the USA (ASRC-CUNY, Memorial Sloan Kettering Cancer Center MSKCC). Her research interests are in the field of AFM for the characterization of nanomaterials and biological entities in liquid environment and with a multiparametric approach.

Mohit Kumar is a La Caixa Junior leader fellow at the Institute for Bioengineering of Catalonia in Barcelona, Spain. His research interests range from supramolecular nanomaterial, dissipative structures to super-resolution imaging and nanomedicine. Mohit holds a Master's degree in Chemistry from Sri Sathya Sai Institute of Higher Learning, India and completed his Ph.D. with Prof. Subi George at Jawaharlal Nehru Centre for Advanced Scientific Research, India. He was a postdoctoral fellow with Prof. Rein Ulijn at the City University of New York.

2. Fluorescence based Super-Resolution Microscopy (SRM)

Fluorescence microscopy has long been used to image structures of various synthetic nanomaterials and biological samples like cells and *in vivo* animal models. The techniques utilize the fluorescence emanating from the sample, either inherently or through external fluorescent dye labelling, to visualize the internal structures. Being an optical method, it can advantageously image samples in their native solution state and at various sample depths. Therefore, it was among the earliest methods to probe dynamic self-assembly processes in solution. But typical fluorescence microscopy is limited in spatial resolution by diffraction limit (Abbe limit, i.e. roughly half the wavelength of exciting light, around >200 nm).[4] However, over the years, the resolution has been significantly enhanced due to the development of new techniques from routine confocal to various SRM, which can provide resolution comparable to conventional AFM and TEM. Furthermore, enhanced speed of imaging has also facilitated recording live videos of dynamic processes. As supramolecular chemistry has increasingly shifted its focus from equilibrium based stable self-assembly to kinetic and out-of-equilibrium self-assembly, it has utilized fluorescence microscopy and SRM to provide detailed insight into the dynamic transformation of nanostructures over time. This section will demonstrate how supramolecular systems have taken advantage of the development of fluorescence imaging techniques to probe dynamic and non-equilibrium self-assembly with increasingly high resolution.

In biology, self-assembly is highly dynamic, where nanostructures continuously form and degrade by consuming chemical fuel. The first example of bio-inspired dynamic self-assembly that forms and breakdown nanostructures in presence of chemical fuel was reported by Boekhoven *et al*.[2c] The design consisted of a non-assembling molecule with anionic carboxylate groups which was coupled to an alkylation-hydrolysis reaction. The alkylation reaction with a fuel resulted in a molecule which can undergo assembly and a competing hydrolysis reaction formed the non-assembled state. The alkylation resulted in the formation of self-assembled nanofibers, whereas spontaneous hydrolysis led to the disintegration of nanofibers. The authors could probe the dynamic formation and degradation of nanofibers in real-time with confocal laser scanning microscopy (CLSM) using Nile red as the fluorescent stain. The *in situ* and real-time visualization of fibre growth, shrinkage, and the overlapping periods during a reaction cycle was crucial in understanding the fuel-driven self-assembly process. It revealed a stochastic collapse of the fibres with rates up to 15 mm/min, reminiscent of the collapse of microtubules in living cells. Such conclusions could not have been possible without real-time imaging. These results suggested that the *in situ* CLSM imaging of the dynamic self-assembly can provide crucial insights into the nanostructure formation and the mechanism of self-assembly.

The above example illustrated the ability of CLSM for real-time imaging, however, it is limited in its spatial resolution. A simple method to enhance spatial resolution in a typical CLSM is by using airyscan technique. The airyscan introduces a unique detector design, consisting of an array of 32 detectors, that collects additional light which is otherwise rejected in a traditional CLSM. Therefore, airyscan based CLSM improves the signal to noise resulting in improved resolution.[5] Kubota *et al*. used high-resolution airyscan CLSM to understand the self-sorting patterns of nanofibers.[6] The chemical reaction between a hydroxylamine and aldehyde to form oxime was used to form self-sorted nanofiber networks. Addition of **1** to an aldehyde containing peptide based hydrogelator **2** resulted in the formation of self-assembling oxime derivative of peptide **3** (Figure 2a). Initial self-assembly of peptide-based gelator **3**, using a suitable fluorescent probe, revealed the formation of nanofibers through the nucleation-elongation process. Preliminary CLSM imaging of peptide based nanofiber assembly in the presence of lipid type hydrogelator **4** showed the formation of interpenetrated self-sorting network as visualized by CLSM imaging. Moreover, using a two-step oxime exchange reaction, the authors could generate a parallel self-sorted network (Figure 2b). *In situ* time-lapse airyscan CLSM studies confirmed the preferential nucleation of peptide type nanofibers near the lipid nanofibers and their elongation along the lipid. Airyscan CLSM imaging was crucial in understanding the formation of distinct interpenetrated and parallel self-sorted network patterns by controlling the kinetics of seed formation.

Another method that has been extensively used in biology for imaging dynamic events like cytoskeleton assembly and vesicle trafficking is total internal reflection fluorescence (TIRF) microscopy. TIRF microscopy selectively excites the fluorophores present at less than 100 nm deep into the sample due to the short penetration distance of the evanescent wave produced at the glass slide-liquid interface because of the total internal reflection of exciting light. This can offer a high signal to noise ratio when compared to CLSM imaging by reducing the background fluorescence from the fluorophores outside the sub-micron surface while observing the dynamic events.[7] Samperi *et al.* used TIRF microscopy to show the complex motion of a molecule along the self-assembled nanostructure by the continuous supply of a stimulus.[8] A three-component gel was fabricated using a cationic imidazole amphiphile, an anionic porphyrin derivative and

10.1002/anie.202208681

a light-responsive anionic azo derivative. The photoisomerization of the azo derivative served as a switch for the movement of the porphyrin molecules over the nanofibers of the imidazole amphiphile. The changes in the relative fluorescence intensity from the TIRF imaging clearly showed the movement of porphyrin molecules along the fibres.

LSM and related optical techniques have been used extensively to image the morphology of nanostructures, however, imaging the mechanical properties variations of self-assembled structures requires a new approach. Cell membrane, which regulates the integral functions for sustaining life, is formed from the self-assembly of lipid molecules. Within a cell, the membrane order and the resultant mechanical property of the membrane plays a crucial role in regulating various cellular and subcellular processes. Thus, an in-detail understanding of the order and the resultant tension of the lipid membranes in living cells is of significant interest. Colom *et al*. have visualized the dynamic changes in the tension within the self-assembled lipid membrane by co-assembling with a fluorescent push-pull molecule termed as fluorescent lipid tension reporter (FliptR, **5**, Figure 2c).[9a] The FliptR molecule was composed of dithienothiophenes and its S, S dioxides as flippers. The application of a lateral mechanical pressure planarizes **5** from its twisted form resulting in a red shift of the excitation wavelength (Figure 2d). Thus, changes in the

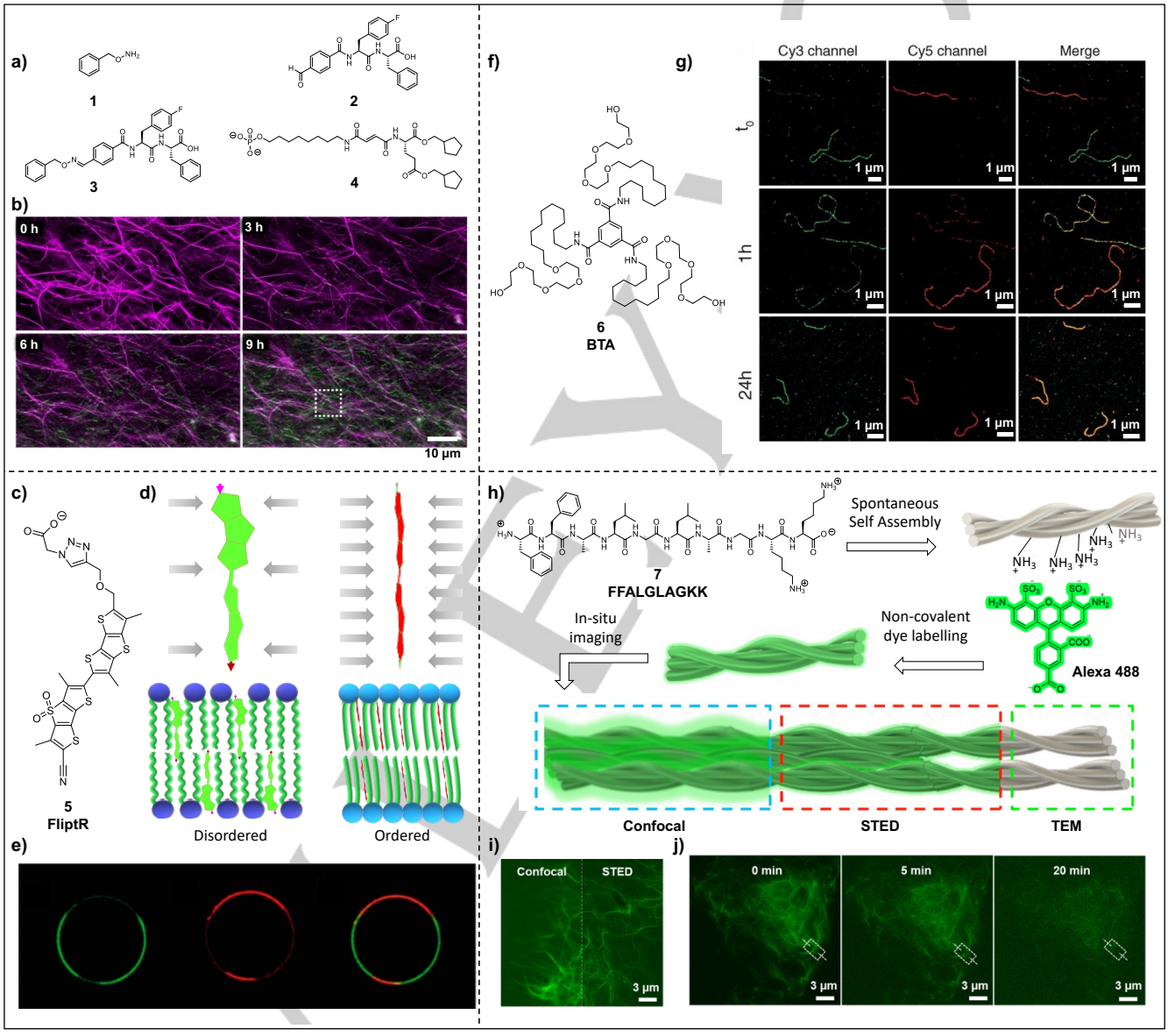

Figure 2. Super-resolution imaging of self-assembly processes. (a) Chemical structures of peptide hydrogelator and lipid molecule and (b) corresponding time-lapse imaging of the formation of parallel self-sorting nanofibers network of **3** and **4**. (c) Chemical structure of FliptR probe **5** and (d) shows that the pressure exerted by lipid vesicles on FliptR probe can planarize the molecule, leading to changes in excitation wavelength as well as the fluorescence lifetime. (e) CLSM imaging of vesicles with different lipid composition containing FliptR probe, which form domains of disordered membrane and liquid-ordered membrane within the same vesicle. The image was obtained by exciting at two different wavelengths (left and centre) and the merged image is presented on the right side. (f) Chemical structure of BTA molecule **6** and corresponding (g) STORM images of Cy5- and Cy3-labeled BTA derivative at different mixing time points. The Cy3 and Cy5 channels along with merged images reveal monomer exchange mechanisms in self-assembly. (h) Schematic showing the self-assembly of peptide **7** and its non-covalent labelling with Alexa-488 dye for STED based SRM imaging. (i) Nanofiber images of self-assembled **7** showing the enhanced resolution of STED compared to confocal. (j) Snapshots of real-time and *in situ* STED video imaging of self-assembled **7** in the presence of enzyme thermolysin, showing that enzymes act directly on fibers to disintegrate the structure. Figures adapted with permission from (a-b) reference [6]. Copyright 2020 Springer Nature; (e) reference [9b] Copyright 2015 ACS; (f-g) reference [12]. Copyright 2014 AAAS; (h-j) reference [25a]. Copyright 2020 ACS.

excitation wavelength of **5** can provide a readout of the mechanical pressure. Co-assembly of FliptR within membranes of higher lipid packing, arising from the highly ordered acyl chains, planarizes the FliptR probe by exerting high pressure. However, lower lipid packing with disordered acyl chains results in low-pressure exertion on the probe (Figure 2d). Additionally, changes in the membrane tension can alter the packing of lipids. Hence, monitoring the changes in the lipid packing can indicate the dynamic changes in the membrane tension. The authors demonstrate that subtle changes in the membrane order of lipid assemblies were accompanied by a significant change in the excitation wavelengths of co-assembled FliptR molecules, making it suitable to visualize membrane tension variation using CLSM microscopy. This was demonstrated with CLSM imaging of lipid vesicle in the presence of FliptR, obtained by exciting at two different wavelengths (Figure 2e, left and center) and the merged image showing domains with different membrane tension (Figure 2e).[9b] The membrane tension changes also resulted in the variation of the fluorescence lifetime of FliptR molecules, which were used to map tension in artificial as well as living cells by using fluorescence lifetime imaging microscopy (FLIM).[9a] FLIM images of cell membranes containing **5** directly imaged the membrane tension as a function of lipid packing. Within *in vitro* study, the fluorescence lifetime of the FliptR increased with increasing membrane tension in HeLa cells and MDCK cells. Thus, *in situ* FLIM imaging provides a unique tool to visualize spatial variations in physical properties like membrane ordering.

The above examples demonstrated the ability of fluorescence microscopy to probe dynamic self-assembly processes. However, the spatial resolution of a conventional CLSM is approximately 200 nm due to the diffraction limit, thus restricting its use in visualizing smaller structures. With the advent of super-resolution microscopy (SRM), the visualisation of nanostructure details, that were earlier imperceptible to the existing visualising techniques, was made possible. Compared to CLSM, SRM is capable of achieving the spatial resolution well below the diffraction limit and thus providing us with nanoscale information of the structure.[10] There are mainly three types of SRM techniques as discussed below in sections 2.1, 2.2 and 2.3.

2. 1. Single Molecule Localization Microscopy (SMLM)

SMLM includes techniques like Stochastic Optical Reconstruction Microscopy (STORM) and Points Accumulation for Imaging in Nanoscale Topography (PAINT). SMLM utilizes dye molecules whose emission can be switched on and off. At any given time, most of the fluorophores are in their off-state and the instrument records the precise spatial positioning of the individual fluorophores in their on-state by considering the centroid of the point spread function. By acquiring a large number of scans, the image of the nanostructure can be reconstructed with spatial resolution below 20 nm.[11] PAINT and STORM techniques differ only in the photo modulation methods utilized to achieve single-molecule illumination. SMLM has the best spatial resolution, but it is a slower imaging technique since it reconstructs an image from a large number of scans.

Lorenzo *et al*. reported the first use of SRM to visualize the dynamics of supramolecular polymers at the individual fibre level.[12] STORM was used in combination with stochastic modelling to study the monomer exchange pathways in self-assembled benzene-1,3,5-tricarboxamide (BTA, **6,** Figure 2f) nanofibers. The studies provided mechanistic insights to confirm a homogenous exchange of monomers throughout the length of self-assembled BTA fibres (Figure 2g). Although the bulk solution studies had provided evidence of exchange dynamics in the supramolecular self-assembly process, this study provided a clear mechanism of the nanoscale dynamics in self-assembly. Additionally, Baker *et al.* demonstrated the influence of chirality in the BTA self-assembly leading to nanofibers with reduced assemblies.[13] STORM was also used to unravel the exchange dynamics of peptide amphiphile nanofiber.[14] Unlike the BTA monomer, STORM imaging in peptides revealed that the dynamic monomer exchange in the self-assembly of peptide amphiphiles is heterogeneous in nature. Visualization using STORM clearly showed the presence of both dynamic domains and inactive domains in the same nanofiber. Owing to its very high spatial resolution and multicolour imaging, STORM has been used for understanding the assembly dynamics of nanofibers. A closely related technique, PAINT has been used to study the dynamics of dipeptide (diphenylalanine) self-assembly which also corroborated the heterogeneous polymerization mechanism, as exchange dynamics as a result of the increased internal order observed in peptide amphiphiles described above.[15] Moreover, PAINT has also been used for the super-resolution imaging of membrane tension in living cells using the FliptR probes discussed earlier.[16]

By taking advantage of the over expressed enzymes on cancer cells, enzyme instructed self-assembly (EISA) phenomena have been utilized in selectively controlling cellular behaviour.[17] Despite numerous examples, the exact mechanisms behind the changes in cellular behaviour during EISA were poorly understood. The traditional CLSM are resolution limited in visualizing the *in situ* dynamic morphological changes occurring inside live cells. Yao *et al*. utilized STORM to monitor the dynamics of the EISA process inside a cell.[18] The supramolecular dynamics of a synthetic tripeptide containing a phosphorylated tyrosine as the enzyme responsive motif was studied inside cancer cells. STORM images probed the dynamic transformation of the precursor molecules into nanofibrillar assemblies in the presence of alkaline phosphatase enzyme in cellular milieu, with up to 50 nm spatial resolution. With overexpressed alkaline phosphatase enzyme at the surface of a model cancer cell, the initial granular assemblies formed at the plasma membrane slowly converted to nanofibers eventually causing cancer cell death. In contrast, the *in situ* visualization of EISA in HeLa cells showed the formation of nanofiber assemblies directly inside the cells, in their native form. STORM studies were crucial in understanding the supramolecular self-assembling mechanisms and pathways of EISA with different enzyme distributions. Even though STORM offers an excellent spatial resolution of up to 10 nm, it requires specific photoswitchable dyes, redox buffer solutions and longer imaging time. Moreover, all the aforementioned STORM imaging is performed on samples taken at various time points instead of real-time, *in situ* imaging, thus limiting its use to probe dynamic processes.

2.2. Structured Illumination Microscopy (SIM)

SIM is based on the generation of interference patterns (moiré fringes) by the nanostructure fluorescence when illuminated with high spatial frequency patterns. Mathematical deconvolution of these interference signals results in a super-resolution image with

a spatial resolution of below 120 nm.[19] SIM is fast and compatible with any fluorescent dye but is limited in resolution.

Compared to STORM, SIM enables the visualization of nanostructures with any standard fluorophores. Sarkar *et al*. have studied the various aspects of multicomponent supramolecular polymerization leading to di-block and tri-block-supramolecular block co-polymers using SIM with a spatial resolution of 120 nm.[20] Deepika *et al*. used SIM for understanding the chiral differentiation in supramolecular polymerization process by visualizing the chirality-driven self-sorting of L/D peptide conjugated nanofibers.[21] These examples have shown that SIM has the potential to image self-assembled structures with very high resolution. However, these microscopic images were snapshots at different time points instead of *in situ* real-time imaging. Although, SIM has been used to visualize real-time dynamic processes in biological and synthetic samples,[22] to our knowledge, there are no reports on the use of SIM for *in situ* real-time imaging of supramolecular self-assembly processes.

2.3. Stimulated Emission Depletion microscopy (STED)

STED employs two aligned concentric laser light beams, where the inner beam excites the fluorophore and a doughnut-shaped outer beam deactivates the fluorophores in the outer regions of the point spread function (PSF). This results in a reduced PSF with emission coming only from the fluorophores close to the centre of the doughnut which in turn enhances the resolution below 50 nm.[23] STED provides the intermediate resolution and the fast-imaging ability to record videos of dynamic processes. Although the SRM was initially used for cellular imaging, now it is increasingly being used to image synthetic self-assembly with unparallel ability.

STED microscopy provides a better spatial resolution than SIM and easy sample preparation, fast imaging capability when compared to STORM. Onogi *et al*. used CLSM and STED SRM to investigate the self-sorting behaviour of a supramolecular multicomponent hydrogel system composed of a peptide gelator and an amphiphilic phosphate gelator.[24] *In situ* imaging of the multicomponent system using confocal microscopy indicated the formation of two distinct fibre networks. The peptide gelator showed heterogeneous formation of fibres in a spatio-temporal manner whereas the amphiphilic phosphate gelator formed fibres immediately confirming the independent growth and self-sorting of the two fibres. However, the evaluation of self-sorting phenomena using Pearson correlation co-efficient of the CLSM images showed a weak correlation between the fibres with a value of 0.30 ± 0.15. Interestingly, STED images showed the formation of distinct fibres with a resolution up to 80 nm and a Pearson co-efficient of 0.15 ± 0.10. The reduced Pearson co-efficient of STED images when compared to that of CLSM images clearly indicated self-sorting phenomena with no correlation between the two fibres. Thus, STED imaging provided clear evidence and quantified the self-sorting process among fibers which were obscured with confocal.

Imaging of supramolecular nanostructures with confocal microscopy and SRM techniques requires fluorescent labelling of the samples. Such labelling is often achieved by covalent conjugation of fluorescent dyes to the self-assembling monomers, which is an expensive task and it can interfere in the assembly process. In order to overcome the issues related to the covalent conjugation of fluorescent dyes, Kumar *et al*. reported a non-covalent attachment of a fluorescent dye to self-assembled peptide for *in situ* SRM imaging using STED.[25] They investigated the self-assembly of a decapeptide **7** consisting of an enzyme responsive motif and two Lysine residues resulting in positively charged nanofiber. Thus, fluorescent labelling of nanostructures could be achieved by simple mixing of a negatively charged fluorescent dye, Alexa 488, to positively charged peptide nanofibers of **7** due to electrostatic interaction (Figure 2h). Since Alexa 488 is a dye compatible with STED microscopy, it was used for the visualization of nanostructures in solution with up to 60 nm resolution (Figure 2i). Furthermore, the addition of a protease enzyme (thermolysin) resulted in the degradation of the peptide nanofibers within an hour which was probed in real-time (Figure 2j). The *in situ* STED imaging provided visual confirmation regarding the direct action of the enzyme on the self-assembled nanostructures rather than acting on the disassembled peptide monomers. The simple addition of dye to the pre-assembled nanostructure is a very convenient labelling method and it was shown to be applicable to a range of cationic peptide assemblies. Hence, this strategy can potentially be used for SRM imaging of a variety of positively charged self-assembled nanostructures.

Therefore, we show that fluorescence based confocal and SRM techniques provide the ability to study the dynamics of simple to complex supramolecular nanostructures that were not achievable by the traditional ensemble studies. *In situ* real-time imaging using SRM techniques will help in the development of new functional materials by unveiling their nanoscale structural dynamics in solution.

3. Solution State Atomic Force Microscopy (SS-AFM)

AFM constitutes an ideal setup for the visualization of self-assembled nanostructures, given its very high spatial resolution, which is typically less than 10 nm in the lateral dimension (in *x* and *y*) and less than 0.1 nm in the vertical dimension (in *z*). AFM is the only technique which can provide information about the height and therefore build the three-dimensional topography of the sample, an information which can only be indirectly obtained with other techniques. A schematic of the AFM, showing its main components, i.e. the scanners for the movements in the three directions, the cantilever terminating with a sharp tip and the laser method for recording the sample topography, is shown in Figure 1. AFM has been one of the routinely used techniques to image supramolecular nanostructures. But AFM imaging has been performed mostly on dry samples which fail to capture the temporal evolution of self-assembly. In this section, we will first briefly describe the capability and limitations of dry state AFM in characterizing supramolecular assemblies, followed by the advancements in imaging in liquid environment using SS-AFM. Finally, recent approaches will be reviewed, based on SS-AFM combined with high speed imaging, that facilitate investigation of dynamic self- assembly with much improved temporal resolution.

In an early report, the AFM has been used in contact mode, i.e. while continuously touching the sample surface with a constant force, to visualize the topography of microtubules covalently attached to a silicon substrate, both in dry and in aqueous conditions.[26] It was shown that the image quality in liquid medium can be improved by fixing the microtubules, thus making them

10.1002/anie.202208681

more resistant to tip pressure. In subsequent reports, the tapping mode AFM has been used to image different supramolecular structures (toroids, helicoids, fibers), after their complete formation in dry conditions, which provided intricate details of the self-assembled structures below 5 nm resolution.[27] However, as the focus of supramolecular chemistry shift from equilibrium based end point nanostructures to probing temporal evolution of nanostructure, SS-AFM has emerged as a promising technique for probing real-time transformation.

In order to study the dynamics of self-assembly with an AFM, different conditions need to be fulfilled. In particular, it is not only necessary to perform experiments in solution state, but also in situ, observing the evolution of the same set of structures over time. An important requirement is the time resolution of the technique, i.e., the imaging speed should be high enough to follow the evolution of self-assembly process within its characteristic timescales. This timescale depends on the kinetics of the assembly processes under investigation and usually, it is in the seconds or fractions of seconds range.[28] A critical parameter for the real-time imaging of dynamic supramolecular structures is the stable adhesion of the sample on a supporting substrate, i.e. sample/substrate interaction should be strong enough to facilitate imaging, avoiding sample detachment and sample being dragged by the tip during scanning. However, covalent immobilization may not be the best choice in the case of supramolecular structures, as it may affect or limit the self-assembly process under investigation. Additionally, in order to avoid sample damage, the AFM tip-sample interaction forces should be kept as low as possible.[27, 29]

Atomically flat surfaces, like muscovite mica and graphite, are the most commonly used substrates for AFM measurements, due to their smoothness. While graphite is a hydrophobic surface, mica is hydrophilic and its negative surface charge can be used to electrostatically attract positively charged nanostructures from solutions. Chemical modification of mica surfaces, like silanization with (3-Aminopropyl)triethoxysilane [30], or coating with positively charged polymers, like poly-L-ornithine[31], allows adsorption of negatively charged nanomaterials for imaging in dry and liquid state. For imaging negatively charged molecules like DNA, an aqueous solution of divalent cations like $MgCl_2$ are also frequently

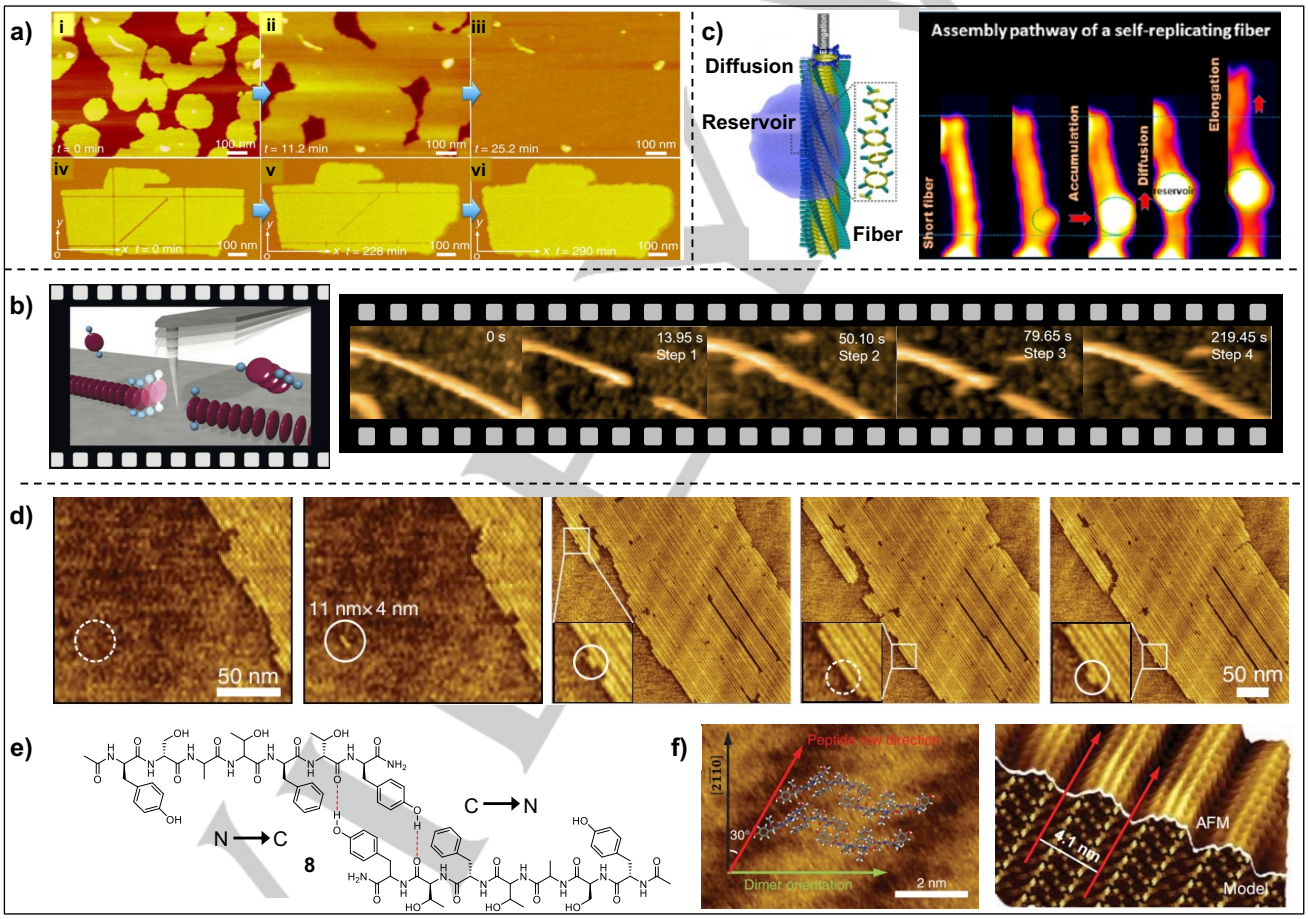

Figure 3. SS-AFM imaging of supramolecular processes in solution. (a) SS-AFM images showing the self-assembly of amphiphilic peptoids forming lipid-like membranes (i-iii) and their self-repair properties (iv-vi). Images are obtained with time resolution of several minutes/frame. (b) Schematic of the tip-induced fabrication and disruption of a supramolecular block copolymer containing Porphyrin derivatives (left image). Images on right side panel show video rate HS-AFM micrographs (rate: 10 frames/s) showing a sequence of nanomanipulation steps performed on the same fiber (step 1: mechanical disruption of a single fiber made with a Porphyrin derivative via the AFM tip; step 2: insertion of a second Porphyrin derivative and formation of a supramolecular block copolymer; step 3: UV irradiation (λ=365 nm) and selective etching of the portion containing only the second Porphyrin derivative; step 4: fiber regeneration by addition of a different Porphyrin derivative containing a photoradical generator. (c) Schematic illustration of the mechanism of the supramolecular polymerization of an oligopeptide into a fiber made with repeating hexamers (left image) and corresponding HS-AFM images of a single growing fiber (rate: 10 frames/s) in aqueous medium. (d) Set of HS-AFM images (time resolution: few seconds), showing the formation of a self-assembled array made up of dimers of oligopeptide **8** on MoS_2 and (e) chemical structure of oligopeptide 8. (f) Overlap of the most stable dimer conformation with the high-resolution AFM image (left image). Simulated AFM image of peptide rows (right image) along their preferred orientation on MoS_2 was consistent with 3-dimensional AFM data. Figures adapted with permission from (a) reference [33]. Copyright 2016 Springer Nature; (b) reference [28b]. Copyright 2018 John Wiley and Sons; (c) reference [28c]. Copyright 2020 ACS; (d-f) reference [28a]. Copyright 2018 AAAS.

used here, the positive ion acts as a bridge between the mica surface and the molecule to be adsorbed. Furthermore, less common methods use lipid bilayers coated mica as substrates for the adhesion of different molecular aggregates.[32]

Once the sample preparation is optimized, the most adequate AFM mode for solution state imaging is the tapping mode. Here, a periodic oscillation of the cantilever is externally excited and variation of this oscillation is detected by the laser to track sample topography. Tapping mode can produce more gentle forces on the sample compared to the contact mode, as the tip only intermittently contacts the sample.

The tapping mode SS-AFM imaging has been used by Jin *et al.* to study the self-assembly of lipid-like peptoids forming two-dimensional membranes on a mica substrate.[33] In this work, the stability and growth of membrane patches were studied over a few hours in water and in various aqueous buffer. Moreover, the time evolution of the membrane growth till their coalescence into a continuous single layer, over tens of minutes, was imaged *in situ* (Figure 3a, i-iii). Due to the advantage of AFM to probe height, an increase in membrane thickness could be probed in real-time. The authors probed the self-repairing capability of membranes in real-time using SS-AFM demonstrating that the membranes repair faster along one axis compared to the other, confirming the anisotropic growth process (Figure 3a, iv-vi). Such mechanistic insight into the self-healing process and probing the dynamic change in membrane thickness was not possible to obtain with other techniques. Ashwanikumar *et al.* used SS-AFM to visualize the disassembly process of various cell penetrating self-assembling peptides that form nanotapes.[34] SS-AFM imaging of the disassembly process in real-time revealed that nanotapes disassemble in a layer by layer fashion resulting in a gradual decrease in thickness. The above example demonstrates the potential of SS-AFM for probing self-assembly and disassembly *in situ*. In both the above-mentioned works, the assembly processes were studied within the timeframe of standard AFM imaging (several minutes/frame) and thus the technique was used only for imaging slow processes in self-assembly.

In order to push the time resolution of the technique, fast AFM setups are nowadays available, based on tapping mode imaging. Fast AFM provides simultaneous high speed and high resolution imaging, thus reaching single molecule resolution (high speed AFM, HS-AFM). These setups feature dedicated components, namely small scanners and small cantilevers that have been originally developed in customized AFMs for the live imaging of biological processes under physiological conditions.[35] In these instruments, the acquisition time of one image is less than a second and can reach the millisecond (ms) range.

HS-AFM has been used to image nanostructures with up to 100 ms temporal resolution. For example, a custom-made HS-AFM was used to probe the hybridization of a protein-single stranded DNA complex on mica surface. Imaging of 13 nm long protein-DNA complex was obtained in an aqueous buffer containing $MgCl_2$ to improve adhesion of complex on mica via electrostatic interactions. Such high speed SS-AFM revealed the high lateral mobility (tens of nanometer) of protein-DNA complex and stochastic fusion of structures within 100 ms time frame. *In situ* probing of such fast dynamic behaviour could only be possible due to the fast scanning capability of HS-AFM.[36]

Custom-made HS-AFM setups have also been used to visualize dynamic aspects of supramolecular polymerization in completely synthetic systems.[28b, 28c] For example, Fukui *et al*. probed the assembly of a porphyrin derivative into fibers in methylcyclohexane.[28b] Here, graphite was found to be a suitable substrate for stable adsorption and growth of fibers. The authors report HS-AFM imaging at 10 frames/sec (video rates), visualizing the real-time growth of fibers by the addition of monomers from the solution and self-repairing properties (Figure 3b). From the analysis of HS-AFM images, the growth rate was found to be very similar to the value obtained in solution (12.4 $nm{\cdot}s^{-1}$ corresponding to 35 porphyrin $units{\cdot}s^{-1}$). Furthermore, the authors performed nanomanipulation of a single fiber strand (Figure 3b), either by cutting it with the AFM tip or by selectively photoetching a segment of the nanofibers which consisted of a UV light dissolvable porphyrin unit. The overall result is the dynamic formation and disruption of a supramolecular block copolymer on demand. The whole manipulation of individual fibers could be video imaged in real-time with HS-AFM, where the AFM tip was also involved in the process of fiber disintegration.

Recently high speed features are integrated into commercial AFMs. Maity *et al*. used one of such systems to probe the mechanism of the formation of hexameric macrocycles that autocatalytically self-assemble into fibers.[28c] Using HS-AFM imaging of single fibers at the rate of 0.5 frames/s, they hypothesize a mechanism where precursor aggregates as trimer, tetramer and hexamer macrocycles, accumulate and diffuse along one-dimensional fibers, to deliver monomers to the growing fiber ends (Figure 3c). The proposed mechanism was also supported with molecular dynamics simulations. Thus, the hypothesis of the growth mechanism could be confirmed by direct observation in real-time with HS-AFM, which could otherwise only be inferred with various other indirect measurements. Experiments were performed in aqueous buffer on a mica substrate covered with a lipid bilayer to improve fibers immobilization and provide sufficient degrees of freedom for their growth. Chen *et al*. performed video imaging of the self-assembly of an oligopeptide array on Molybdenum Disulphide (MoS_2) surface.[28a] The chosen oligopeptide **8**, which has a high affinity for MoS_2 substrate, adsorbs as dimer at specific locations in the crystallographic lattice of MoS_2 (Figure 3d, e). The authors used *in situ* HS-AFM to image real-time growth of two-dimensional arrays of peptide self-assembly. Through molecularly resolved images, they demonstrated that the two-dimensional array is formed one row at a time. Therefore, since the two-dimensional growth happens by forming one-dimensional rows at a time, it does not require a critical size of nuclei that grow spontaneously, which is otherwise essential for traditional two-dimensional nucleation-growth processes (Figure 3d, f). Such molecularly resolved images obtained at time interval of a few seconds in aqueous medium provided insights into two-dimensional nucleation-elongation process that could have been lost with dry state imaging as well as at slower imaging rates.

4. Liquid Phase Transmission Electron Microscopy (LP-TEM)

TEM utilizes the transmission of electrons through samples for imaging matter down to the atomic level. The resolution of a microscope is roughly half the wavelength of the illumination source.[37] Since the wavelength of electrons is much smaller than the wavelength of light, TEM can image materials with spatial resolution of less than 1 nm. TEM has extensively been used in

the last decades to image a myriad of supramolecular nanostructures with molecular and atomic resolution. One of the requirements for TEM imaging is that the sample must be kept under high vacuum conditions. Samples under high vacuum conditions mean that standard TEM imaging can only be performed on non-volatile materials. This limiting feature forces specimens to be dehydrated before imaging. However, sample dehydration fails to capture the dynamic processes involved in supramolecular systems that self-assemble over time. Rapid cryo-cooling of samples in a thin layer of vitrified water, known as cryogenic TEM (cryo-TEM), arose as an alternative for sample dehydration problems.[38] Even with cryo-TEM, some questions remained, like how to generate the underlying 3D structure from the acquired images. Despite the initial obstacles, cryo-TEM has advanced tremendously in the last three decades.[39] However, as mentioned above, cryo-TEM requires vitrification of supramolecular structures and therefore poses limitations when screening the evolution of self-assembly over time.

In recent times LP-TEM has emerged as a promising technique for *in situ* imaging of nanostructures in their native liquid state[40] with the possibility of visualizing dynamic processes. One of the major successes of LP-TEM is that the liquid sample under investigation is not exposed directly to high vacuum but is efficiently sealed in a liquid cell.[41] Thus, the sample in LP-TEM is under ambient pressure and temperature in solution, which facilitates real-time monitoring of the evolution of supramolecular structures. LP-TEM can also be used to probe biological samples like live cells, which are prone to damage under the high vacuum environment of conventional TEM. This section will first present various types of liquid cells currently used, and special operating conditions, followed by examples of supramolecular self-assembly which have used LP-TEM to visualize the transformation of nanostructures in real-time *in situ*.

The main difference between a LP-TEM and a regular TEM is its liquid cell sample holder. Liquid cells are composed of a top and bottom electron transparent window, usually made of silicon nitride (SiN), graphene, or a combination of both to withstand high vacuum without scattering electrons and loss of solvent media. The most used liquid cell involves two SiN microchips (Figure 4a) that enclose circa 1 to 1.5 µL of the liquid sample and then the liquid cell is sealed. This methodology also enables the flow-in of other media or samples which is particularly important for the real-time study of dynamic events upon application of external stimuli, such as pH and temperature changes (Figure 4a). As mentioned above, instead of SiN, graphene can also be used to create graphene liquid cells, providing a thinner liquid space than those achieved by SiN windows (Figure 4c). This reduced thickness leads to less electron scattering, thus, higher resolved features compared to other methods. The third methodology is a combination of the previous two and consists of a SiN microchip sealed by a graphene sheet (Figure 4b). This method is used to reduce the thickness of large samples such as whole cells allowing the graphene to adapt to the shapes of the objects in the solution. In general, the use of graphene also provides an enhanced protection against beam damage.

The main challenge when performing LP-TEM is to manage the high-energy electron beam which can induce undesired artifacts in the sample. It is possible to reduce the electron dose by employing a direct detection device i.e. camera (e.g. DDCs),[42] that operates in low dose mode, and high speed imaging with high detective quantum efficiency (DQE). Low exposure times and the need for fast imaging conditions to capture sample dynamics add further undesirable effects that translate into low sample contrast. Tailored image analysis methods are very much needed in order to restore original images and unveil structural details that otherwise are not visible in raw images due to low signal to noise ratio. An alternative method is to operate the microscope in scanning TEM (STEM) mode. In STEM mode the beam is focused on a small area (~1 nm) and raster the sample without applying a constant flux in the field of view, such as in TEM mode. It is also reported that the electron dose causes a significant decrease in the pH of aqueous solutions in LP-TEM experiments. Hence, it is crucial to also consider the effects of the decreased pH while planning LP-TEM investigations.

Having described the instrumental details and experimental conditions appropriate for LP-TEM, we present various examples of *in situ* visualization of the self-assembly process. Metal-organic frameworks (MOFs) consist of organic molecules linked together by metal ions to form porous self-assembled structures and are used for application in catalysis, gas storage, sensing etc.[43] The structure of MOFs has been extensively investigated in their crystalline state using electron diffraction techniques like single crystal x-ray diffraction. However, these techniques fail to provide information about the early stage of nucleation and growth processes of individual crystallites. LP-TEM has been used to obtain structural and dynamics of formation of individual MOF crystallites. Patterson *et al*. have used *in situ* LP-TEM to visualize, for the first time, the dynamic nature associated with nucleation and growth of macromolecular MOFs.[44] The precursor solution containing Zr (IV) metal ions and 1,4-benzenedicarboxylate organic linker were injected into a silicon nitride (SiN) membrane-based liquid cell. The silicon nitride chips were plasma cleaned which enhanced the chip hydrophilicity and hence adherence of nanostructures onto the *SiN* surface. This resulted in low sample mobility and consequently enhanced resolution. To study growth kinetics, a flow cell experiment was proposed, and the precursor solution was constantly flowed into the liquid cell during imaging. Initially, particles of 15 nm diameter were observed which grew to around 50 nm in 11 minutes, as screened through video imaging by LP-TEM. Thus, real-time visualization confirmed that the growth of particles does not occur via coalescence but rather through the growth of smaller subunits in solution. The same group also reported the formation and *in situ* visualization of metal organic nanotubes via LP-TEM.[45] In this case, the nucleation and growth of nanotubes could be visualized at high temperature (85 °C) by heating the liquid cell (Figure 4d). Authors observed no adverse effect of the electron beam on the self-assembly process. However, they confirmed that the anisotropic tubular growth is thermodynamically driven, and the size distribution is affected by the *SiN* surface treatment. Treating the observing windows surface has an effect on whether the enclosed specimen is located in the bulk, onto the chip or in a close by reduced mobility interfacial area. Such mechanistic insight into the growth of crystalline particles and tubular bundles in the above two examples could not have been possible using standard, static TEM imaging.

Having probed the formation dynamics of crystalline materials like MOFs, LP-TEM has more recently been used for live imaging via video acquisition of the dynamic transformation occurring in soft supramolecular nanostructures. Parent *et al.* used LP-TEM to image and understand the dynamics of micelle assembly. As a

10.1002/anie.202208681

WILEY-VCH

REVIEW

proof of concept, the authors studied the assembly process and formation of phenyl-*b*-peptide-*co*-hydroxyl block copolymer micelles *in situ*.[46] The fusion of the individual micelles as well as their morphological transformations starting from their building blocks are crucial in the formation of micelle self-assembly. *In situ* visualization of the process(es) involved in micelle self-assembly clearly demonstrated that the micellar fusion phenomena start with the movement of two random micelles and their interaction to form a larger fused micelle. Along with fusion process, the authors also confirmed the simultaneous unimer attachment as a mechanism for micellar growth. Altogether, LP-TEM provided a useful tool for the direct visualization of the complex nanoscale dynamic processes involved in micellar self-assembly.

More recently Duro *et al.* reported an investigation on oxidation-sensitive supramolecular micelles and vesicles employing LP-TEM among other techniques.[47] The samples were obtained by polymerization-induced self-assembly of the N-carboxyanhydride precursor of methionine using poly(ethylene oxide) as a stabilizing and hydrophilic block to form wormlike micelles, vesicles and gels. Reactive radical species have been reported to form in aqueous media upon electron beam irradiation.[48] This feature allowed Duro *et al.* to use LP-TEM as a tool to i) degrade the vesicles forming polymer using the electron beam, and ii) visualize in real-time the vesicle degradation process as shown in Figure 4e.

The use of LP-TEM for imaging the self-assembly process of small molecules, aside from polymers has been challenging due to the sample sensitivity to electron radiation. Gnanasekharan *et al*. have reported a methodology involving the use of the electron beam in a pulsed fashion. In this way, the electron beam is turned on for one second and then subsequently turned off for ten seconds, with the aim of avoiding sample structural damage that

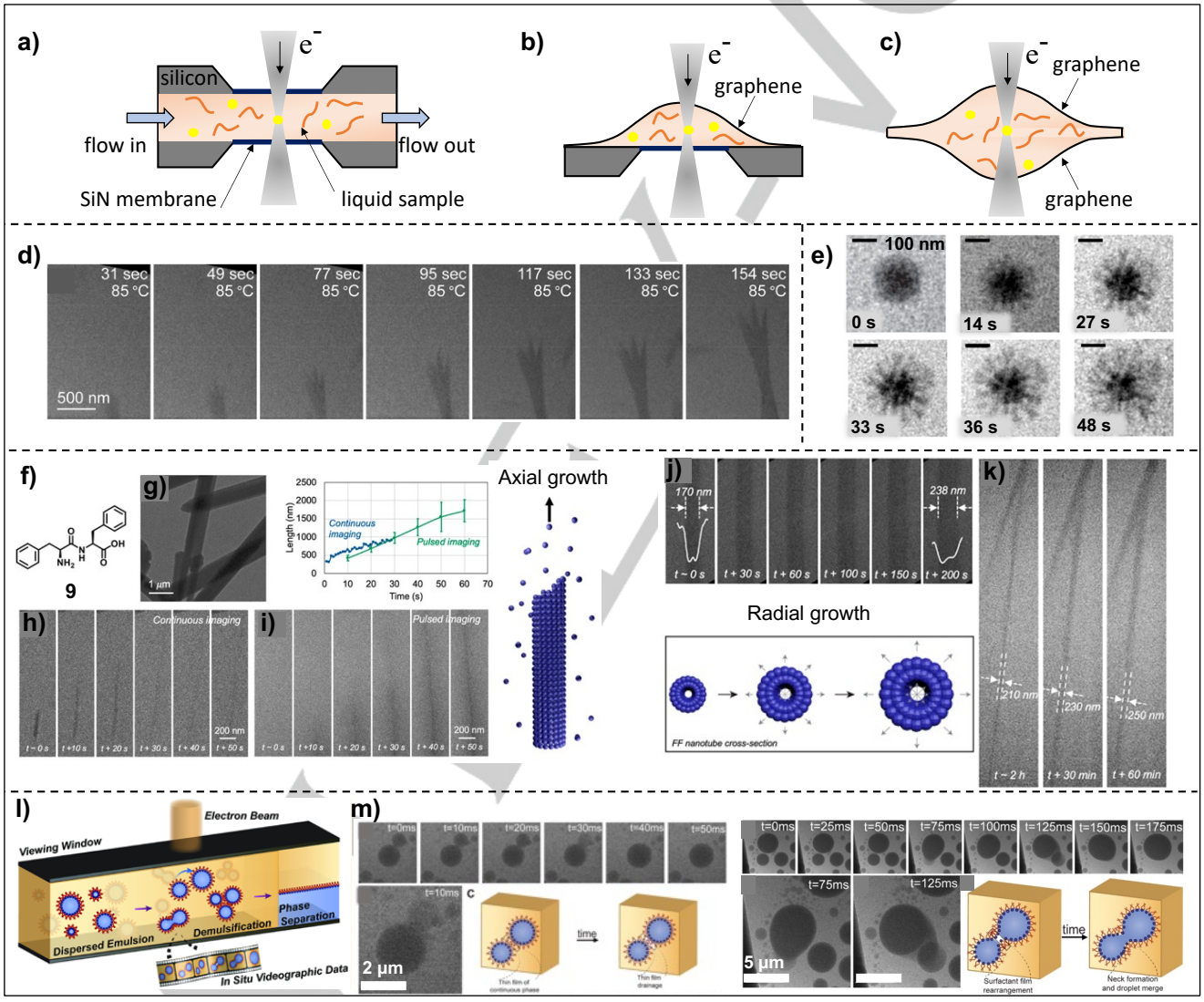

Figure 4. LP-TEM imaging of dynamic self-assembly processes. Schematic of (a) standard liquid cell where sample is sandwiched by two SiN chips with inlet and outlet channels for liquid flow, (b) combination of SiN chip enclosed with graphene sheet, and (c) two graphene sheets forming a graphene liquid cell. (d) LP-TEM micrographs showing nucleation and anisotropic growth of MOF nanotubes as a function of time. (e) *In situ* real-time degradation of methionine-based polymeric vesicles by using the electron beam in liquid STEM. (f) Chemical structure of diphenylalanine dipeptide and (g) the dry state TEM image of its self-assembly; comparative imaging of the nanotubular growth of the dipeptide in (h) continuous and (i) pulsed imaging mode demonstrating linearity in the elongation and impeded growth in continuous imaging mode, confirming advantages of pulsed imaging. Right side panel shows the schematics of axial and radial growth of dipeptide nanotubes and (j-k) shows real-time images of radial growth of nanotubes. (l) Schematic illustration and (m) real-time *in-situ* LP-TEM images of emulsion formation and various steps involved leading to demulsification. Figures adapted with permission from (d) reference [44]. Copyright 2015 ACS; (e) reference [47]. Copyright 2021 ACS; (f-k) reference [49]. Copyright 2021 ACS; (l-m) reference [50]. Copyright 2022 ACS.

is typically caused by continuous imaging.[49] The authors used LP-TEM to monitor the assembly pathways of diphenylalanine dipeptide **9** (Figure 4f, g). Sample solution was injected into the liquid cell and then heated up to 80 °C, followed by a slow cooling ramp inducing structure formation that could be observed in real-time. The imaging revealed the growth of peptide nanofibrils through monomer addition to the fibrillar ends by intermolecular interactions at a rate of ≈20-25nms^{-1} leading to diphenylalanine nanotubes (Figure 4h). Comparison between continuous and pulsed imaging revealed that continuous exposure to the electron beam impedes the growth of nanotubes, whereas pulsed exposure promotes further elongation (Figure 4h-i). This confirms the advantage of using an electron beam in a pulsed fashion for LP-TEM. Furthermore, for the first time, the radial growth profile of diphenylalanine nanotubes was observed, where monomers attach perpendicular to the tubular axis to increase the width of the tube (Figure 4j-k). The same group also used LP-TEM to probe the emulsion formation of sodium salt of dioctyl sulfosuccinate and its demulsification in real-time.[50] Most emulsions are studied in the bulk using light scattering methods which does not provide the mechanism of transformation over time. The reported investigation on emulsion using LP-TEM was able to screen the various pathways involved in emulsion formation like coalescence, Ostwald ripening and flocculation for emulsion evolution towards phase separation (Figure 4l, m).

It becomes clear that the LP-TEM offers tremendous opportunity for *in situ* and real-time imaging of dynamic self-assembly processes with high spatial and temporal resolution. However, the technique is still in its nascent stage, further development in liquid cell design, as well as liquid holders, robust image processing methods, or thorough investigations on electron dose tolerance for samples in liquid water as opposed to vitrified water, are still needed to name a few. However, even with these caveats, LP-TEM is able to deliver an unprecedented understanding of the structure and dynamics involved in self-assembly processes in liquids.

5. Molecular Dynamics (MD) Simulations

Although significant advances have been made in various microscopic techniques to visualize the growth mechanism and dynamics of supramolecular polymers, it is still difficult to capture the events at a molecular resolution (< 20 nm). MD simulations can provide access to the molecular level events under experimentally relevant timescales and conditions (solvents and temperature).[51] Among many supramolecular building units,[52] benzene-1,3,5-tricarboxamide (BTA) has been extensively studied experimentally in both organic and aqueous medium.[53] Consequently, a significant body of computational work has been carried out on this system to understand the dynamic assembly of archetypical supramolecular unit.[54] In this section, we delineate the insights obtained into the dynamic assembly of BTA supramolecular polymers using MD simulations. The insights drawn from the BTA system are expected to be applicable to a wide range of one-dimensional supramolecular polymers.

Early computational studies by Bejagam *et al*. focussed on understanding the cooperative assembly of the BTA appended with alkyl chains in an apolar solvent and the monomer-supramolecular polymer dynamics using all-atom and coarse-grained MD simulations.[55] It was observed that the supramolecular polymers in apolar solvents are highly ordered due to the directional three-fold hydrogen-bonding. To understand the exchange dynamics of alkyl BTAs, Bochicchio *et al*. utilized Well-Tempered-Metadynamics (WT-MetaD) simulations,[56] a method known to capture rare events in molecular systems.[57] A 24-mer stack of BTA with hexyl side chains (**10**) (Figure 5a) was preliminarily equilibrated in *n*-pentane solvent *via* all-atom MD simulation. A monomer exchange from the central region of such a stack was activated using WT-MetaD simulations. The free energy profile for monomer exchange exhibits a two-step process; i) creation of a local breakage/defect (point B Figure 5b and c) in the graph, with structural distortions corresponding to a local minima, and ii) subsequent leaving of the monomer (point C in the Figure 5b and c). The energy penalty for the creation of the local defect followed by the exchange of monomers with the bulk relies heavily on the medium (alkane solvent versus gas phase). This suggests that the monomer exchange can occur *via* both the ends of the polymer/oligomer (bonded to only one monomer) or the bulk of supramolecular polymer (in which any given monomer is bonded to two other monomers on either side).

Given the similarity of one-dimensional supramolecular polymers with the biological filamentous structures (actins, amyloid fibres, etc.) and their application in biomaterials, a large body of work has been dedicated to supramolecular polymers in water.[58] Here, the principle molecular design of BTA based supramolecular building blocks is as follows: i) the central core of benzene-1,3,5-tricarboxamide to act as the source of intermolecular hydrogen bonding, ii) an alkyl chain of appropriate length (twelve carbons) on the amide to protect the hydrogen bonds from interaction with water, and iii) oligoethylene oxide groups at the end of alkyl chains to render the molecules water soluble (**6**, Figure 2f).[59] The first all-atom MD simulation in explicit water for the BTA system was carried out by Baker *et al*.[13] They constructed a stack of 48-mer and optimized it in the gas phase to obtain an initial geometry for the MD simulations. The highly ordered gas phase optimized geometry was subjected to 300 ns of MD simulation and the final 100 ns of equilibration was used to derive structural parameters. In such a simulation two prominent events were observed; i) in the initial stages of run, collapse of the side chains on to the fibre occurs to reduce the hydrophobic interaction with the water (primary folding). However, this still allows water molecules to access some of the hydrophobic domains, ii) to avoid the latter, the fibres tend to deviate from the linear, extended structure to one with folds, reminiscent of secondary folding in proteins (Figure 5d). To check the validity of the obtained structures, the authors computed the small angle X-ray scattering profile from the geometry obtained after equilibration. The simulated X-ray profiles match very closely with the experimentally observed ones. Thus, suggesting that water soluble BTA fibres are not perfectly linear or extended, rather they exhibit collapsed and folded domains. This is in sharp contrast to alkyl substituted BTAs (**10** or its analogues) in organic solvents, which exhibit highly ordered and linear fibre structure. Also, it is worth noting that a small fraction of water molecules does penetrate into the fibre, demonstrating their active role in the assembly process. If not for MD simulations, visualizing the role of solvent molecules in the formation of self-assembled structures is not achievable currently by other techniques.

10.1002/anie.202208681

Although the above elaborated all-atom MD simulations capture the actual interaction between the monomers effectively, the supramolecular polymerization process (going from a pool of monomers to fibres) cannot be accessed due to the larger timescales involved. To study such large timescale (microseconds) events in MD simulation, Bochicchio *et al*. have developed a coarse-grained MD simulation model based on the MARTINI force field.[60] In the coarse-grained model, a group of similar atoms are represented by a single unit (bead) capturing their essential interactions (Figure 5e). Such a process significantly reduces the number of particles and increases the time step in MD simulation to sample microsecond timescale events. The developed model was validated by comparing the key structural parameters and binding energies with those obtained from all-atom simulations. The coarse-grained model reveals that; i) starting from a randomly dispersed monomers, initially (20 – 30

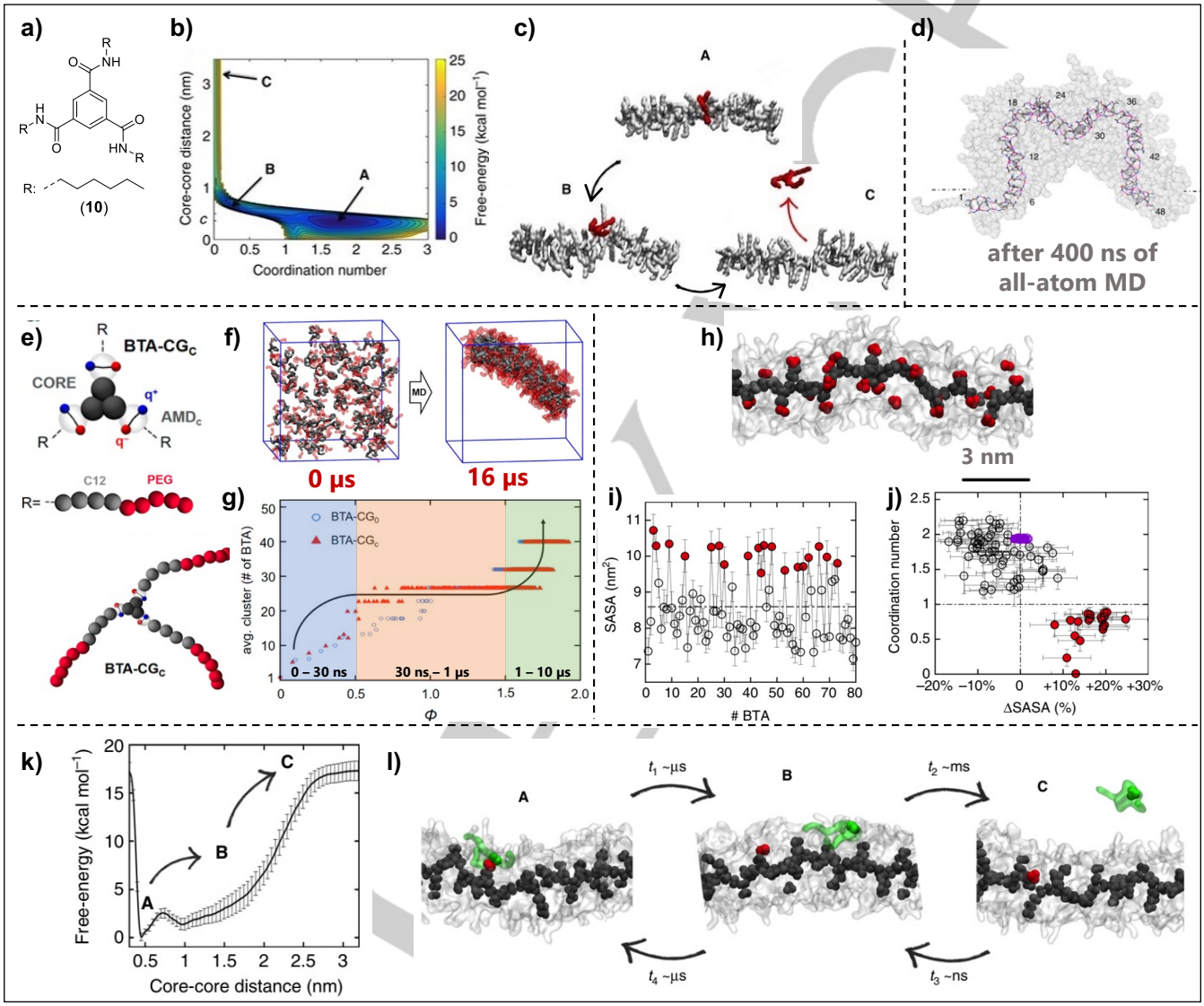

Figure 5. MD simulations to study the dynamics of supramolecular systems**.** a) Molecular structure of benzene-1,3,5-tricarboxamide (BTA) with hexyl side chains (**10**). b) Free-energy profile for monomer exchange of **10** in *n*-pentane as a function of distance between the activated monomer and other molecules in the 24-mer. Here coordination number refers to the number of hydrogen-bonded neighbours of any given molecule. Any given molecule inside a 24-mer has two neighbours on either side, thus leading to the most stable state with coordination number of 2. c) Stepwise exchange process. The monomer depicted in red is activated via WT-MetaD from the central of the fiber. Here 'A', 'B', and 'C' correspond to the different stages of monomer exchange. d) Snapshot of the fiber after 400 ns of all-atom MD of **6** (from Figure 2f) in water. The atoms in the BTA core are represented by different colors and the amphiphilic part is shown in light grey. e) MARTINI-based coarse-grained models of **6**. The central core is depicted by three grey beads, the amide groups are depicted by a dipole (red and blue charges), each light grey bead in the side chain represents three methylene units, and red beads represent PEG. f) Snapshot of the starting and equilibrated structures for a system of 160 BTAs. In the equilibrated snapshot (16 µs), only the largest cluster (85-mer) formed during coarse-grained simulation is shown. g) Trajectory of coarse-grained simulations as a function of average cluster size of BTA and the coordination number (φ). The three coloured regions depict the different timescales during which the fibers evolve. h) Equilibrated structure of **6** in water obtained via coarse-grained simulations. The BTA core is depicted in dark grey and the amphiphilic side-chains are shown in transparent grey. The BTAs at the defect sites ('hot spots') are depicted in red (core). i) Solvent accessible surface area (SASA) as a function of BTA unit in the fiber. The red solid circles correspond to monomers at the defect sites. j) Correlation between the coordination number and the difference in SASA (deviation from the average monomer SASA). The red solid circles correspond to monomers at defect site and the ones in black circle correspond to the monomers in the fiber. The purple data points correspond to BTA (**10**) fiber in organic solvents. k) Free-energy profile of a monomer exchange with the solvent (water) as a function of the distance between the activated core and the other cores in the fiber, obtained via WT-MetaD simulations. l) Snapshots depicting the different phases of monomer exchange along with the corresponding timescales. Figures adapted with permission from (b-c) from reference [56]. Copyright 2017 Springer Nature; (d) from reference [13]. Copyright 2015 Springer Nature; (e-g) from reference [60]. Copyright 2017 ACS and (h-l) from reference [56]. Copyright 2017 Springer Nature.

ns) disordered clusters with 20 – 30 BTA monomers are formed, ii) thereafter these clusters reorganize to form more ordered oligomers, as evidenced by the increase in coordination number (φ), and iii) finally, these ordered oligomers undergo fusion to give rise to larger fibre/polymer (Figure 5f and g). The supramolecular polymer (containing 85 BTA units) formed after complete equilibration (16 μs) is not linear or extended, but rather folded or possesses kinks (due to hydrophobic effect) leading to defects along the fibre (Figure 5h). The defects have been quantified by studying two parameters; i) solvent accessible surface area (SASA) of each monomer, and ii) the coordination number (Figure 5i and j).[56] A coordination number of 2 indicates that each monomer is bound to two more monomers (ideal situation) in the fibre and a value ≤1 is classified as a defect. As can be seen from Figure 5i and j, the monomers at the defect site (shown in red filled circles) possess significantly higher SASA than the average monomers and a low coordination number. This indicates that the monomers at the defect sites are weakly bound and easily accessible by solvent molecules. Such defects act as 'hot spots' for the exchange of monomers from the fibre. Further, WT-MetaD simulations with activating the monomers at the defect site ('hot spot') was carried out to study the exchange dynamics of monomers with the solution. The free-energy profile exhibits two minima (Figure 5k), suggesting that the exchange of monomer is not a single step process, rather it occurs *via* a two-step process (A→B→C). In the first step the monomer leaving the hot spot will diffuse to the surface of the fibre (A→B) and consequently the monomer jumps into the solution (B→C) (Figure 5l). The free-energy barrier for the first step is small (~ 2 kcal mol^{-1}), whereas the second step (B→C) has a significantly higher barrier of 10 kcal mol^{-1}.

Qualitatively, the timescale of the first step (μs) is significantly faster compared to the second step (ms). This is in line with the observation of monomer migration from one site of defect to another along the fibre even during unbiased MD simulations and the hypothesis of faster intra-fibre dynamics compared to monomer exchange based on STORM experiments.[12] The process of monomer incorporation into the fibres occurs in the reverse stepwise pathway with slightly different timescales.

Finally, Marco *et al.* have recently developed a generalized coarse-grained model coupled with enhanced sampling and machine learning to study both organic and aqueous soluble BTAs and porphyrin based supramolecular polymers.[61] The generalized model can be used to study the competition between directional (hydrogen-bonding) and nondirectional (hydrophobic) interactions and their influence on the creation or annihilation of defects, which ultimately dictate the exchange dynamics. Thus, MD simulations provide a complementary and molecular level tool to study the exchange dynamics in supramolecular systems chemistry.

6. Emerging Techniques

Apart from the above discussed techniques, there are a few more techniques/methods that supramolecular systems chemistry community should look out for in the future. Below we will briefly point out some of the emerging techniques which have been mainly used in various other fields but hold great promise for supramolecular systems chemistry. i) Wu *et al*. combined the line scanning of confocal with multi-view imaging and SIM super-resolution imaging. Here, fluorescence was simultaneously collected from three objectives placed at three different angles (Figure 6a, b) to capture fluorescence which is usually scattered out. The signal was integrated using reconstruction algorithms to enhance resolution isotropy.[62] This when combined with machine learning led to >10 times enhanced three-dimensional resolution, extended imaging duration by minimized photobleaching and improved sample depth to provide super-resolution imaging. Although the technique was used for imaging cells and animal models, the possibility of extending it to supramolecular systems will open new avenues for fast super-resolution imaging in three dimensions. ii) Apart from fluorescence-based optical imaging, light scattering-based interferometric scattering microscopy (iSCAT) has shown promise in imaging single biomolecules like proteins in solution. iSCAT does not require dye labeling and is solely based on the Rayleigh scattering of light from the macromolecules and its interference pattern with the reflected light (Figure 6c).[63] Lebedeva *et al*. have used iSCAT to probe the self-assembly of synthetic lipids and their micellar growth kinetics in real-time (Figure 6d).[64] Substantial progress was made when Young *et al*. demonstrated that iSCAT imaging could be correlated with macromolecular mass and therefore mass imaging can be performed with spatial and temporal resolution in

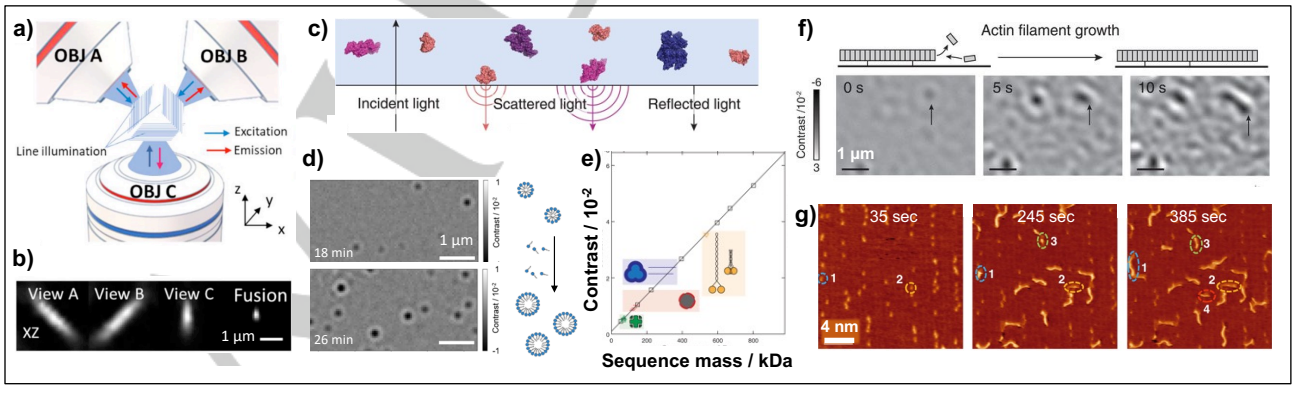

Figure 6. Emerging techniques: (a) schematic illustration of multi-view super-resolution imaging consisting of 3 objectives and (b) the image of a 100 nm bead reconstructed from the signal obtained from three objectives. (c) Schematic representation of working principle of iSCAT and (d) real-time imaging of micelle formation and growth. (e) Ability of iSCAT to predict the molecular mass of different proteins as shown by a linear plot between protein mass and scattering intensity obtained by iSCAT; (f) demonstrates that the iSCAT can probe the real-time growth of actin filaments length as well as provide the change in the mass of the resultant biopolymer. (g) *In situ* and real-time STM images of the growth kinetics of polyethylene polymeric chain on catalytic surface. Figures adapted with permission from (a-b) reference [62b]. (c, e, f) reference [65]. Copyright 2018 AAAS; (d) reference [64]. Copyright 2020 ACS; (g) reference [67]. Copyright 2022 AAAS

solution.[65] By imaging proteins of different mass in solution they showed a clear correlation between the scattering intensity and molecular mass of the protein, validating the ability of iSCAT to image the molecular mass of biopolymers (Figure 6e). This was used for real-time mass imaging of actin filament growth (Figure 6f). Such methods can open doors towards spatiotemporally monitoring the growth of macromolecular mass during supramolecular polymerization. Indeed, attempts are being made in this direction to probe the mass of individual self-assembled particles.[66] iii) Scanning tunneling microscopy (STM) has been used to image nanostructures with molecular level resolution. In recent times, STM was used for real-time visualization of dynamic processes like catalytic ethylene polymerization (Figure 6g)[67] and nucleation-elongation of two-dimensional dynamic covalent polymerization in ambient conditions.[68] These measurements are currently performed at the solid-liquid interfaces and thus limit their use for imaging dynamic processes in bulk solutions. However, future optimization of the technique could potentially provide molecular level details for supramolecular systems in 3-dimensions.

7. Conclusions and Future Directions

As supramolecular chemists continue to seek inspiration from nature, they have been developing self-assembled nanostructures with increasing complexity. Consequently, the focus is gradually shifting away from developing equilibrium-based structures which do not change over time towards kinetically controlled, dynamic nanostructures. Hence, the complete characterization of such dynamic systems cannot be performed by traditional techniques like dry state AFM, TEM, resolution limited confocal microscopy etc. Instead, dynamic supramolecular systems demand real-time visualization of nanostructures as they adapt and reconfigure. In this Review, we have highlighted examples of supramolecular systems which have utilized state of the art techniques for effective probing of dynamic self-assembly in solution, in real-time and *in situ*. The Review is divided into five sections based on the visualization techniques into i) fluorescence based super-resolution microscopy; ii) solution state AFM (SS-AFM); iii) liquid phase TEM (LP-TEM); iv) molecular dynamics (MD) simulations and finally, iv) we have presented a list of emerging techniques which may well offer great potential in characterizing supramolecular systems in the near future. The presented examples clearly demonstrate that the above-mentioned solution-based visualization techniques have provided much-needed insights into the self-assembly process, which could not have been possible otherwise. We have summarized the various features and advantages/limitations of these techniques in Table 1.

It is without a doubt that much progress has been made, but further development needs to be done to meet the requirements of the new generation of dynamic nanomaterials. Below we present the challenges and future directions of the four main visualization techniques discussed in this Review.

7.1 Fluorescence based Super-Resolution Microscopy

The progress made with several optical SRM techniques like STORM and STED has enabled us to visualize dynamic self-assembly in solution in real-time with a resolution close to 10-20 nm. However, it is still not considered a go to technique for supramolecular systems as evident from the very limited examples where dynamic processes are visualized using SRM. There are several challenges like requirement of specific type of dyes for different techniques, long imaging times for techniques like STORM, sample movement in solution etc. These challenges can be tackled by i) the use of label-free imaging methods like iSCAT to avoid dye requirements; ii) the use of advanced reconstruction algorithms and machine learning methods for fast and directed imaging with minimum photobleaching; iii) use of chemically modified sample cells to restrict movement of nanostructures. In the future, the combination of STED and STORM within a single platform might provide us with the best of both i.e., the higher temporal resolution of STED and enhanced spatial resolution of STORM.

7.2 Solution State AFM

A unique feature of AFM is that it is possible to obtain spatially resolved maps of different physical properties of samples, like mechanical and electric properties[69], simultaneously with the sample topography. This can be achieved by recording different other observables like the phase lag of the oscillating cantilever[70] or adding multiple excitation frequencies to the measurements.[71] Also, force versus distance curves can spatially map surface parameters, like stiffness or elasticity.[72] This approach, called multiparametric AFM, has not yet been applied to supramolecular structures and would allow visualizing the changes in the material´s properties, along with topographical changes, during the self-assembly. Thus, multiparametric AFM can open doors to visualization of transient emergence of novel properties in materials, like electrical or mechanical, during the self-assembly process which is otherwise lost in the end point analysis with regular AFM. Finally, correlative experiments can also be performed by combining the SS-AFM setup with other techniques like Tip-enhanced Raman spectroscopy (TERS) and AFM-infrared (AFM-IR), thus combining the high spatial resolution of an AFM together with chemical sensitivity.[73] Nowadays, commercial AFMs are beginning to integrate lasers and optics for confocal fluorescence imaging (for lower spatial resolution) and near field super-resolution techniques, like TIRF and STED, with higher spatial resolutions.[74] In future, this can also be used to probe supramolecular transformations induced by optical stimuli.

7.3 Liquid Phase TEM

One significant advantage of operating with liquid samples is that their handling can be easily automated and combined with other liquid handling techniques for various chemical analyses. High-performance liquid chromatography (HPLC) and gel permeation chromatography (GPC) can be integrated with the flow-based LP-TEM to achieve full automation and complement imaging with chemical and physical characterization. Other systems such as UV/Vis spectroscopy, refractive index (RI), and multi-angle light scattering (MALS) can also be added for better characterization and in situ detection of any chemical damage caused by the electron beam of LP-TEM. Furthermore, the use of a pulsed-electron source in LP-TEM promises to minimize damage from long exposure to the electron beam significantly. This would also allow fast imaging times without limiting the dose available, thus enhancing LP-TEM as a structural technique that captures

dynamic processes in real-time. More recently, laser light has been incorporated into TEM to melt a vitrified cryo-sample locally and probe structural changes in TEM mode in the molten region.[75] This possibility to shine laser while TEM imaging can be potentially used to visualize light or electron induced supramolecular polymerization processes. Following the imaging process, LP-TEM generates noisy, distorted, and blurred images due to the liquid media and its excess thickness. In this regard, deep learning denoising and deblurring algorithms are needed to restore and recover the images generated by LP TEM. As the liquid cell design, acquisition systems, i.e., camera, and microscope capabilities, are continuously under development, there is also the need for a parallel development in the in-silico post-acquisition image analysis front.

7.4 Molecular Dynamics Simulation

The state-of-the-art classical MD simulations with advanced sampling techniques can capture molecular level events up to microseconds in one-component supramolecular systems. Although generalized force fields with minor parameterization can work well for few systems, it is imperative to benchmark and test the validity of the models when applied to a different class of systems. Given the vast amount of experimental and quantum chemical studies for many classes of supramolecular systems, perhaps it is time to develop machine learning based force fields[76] that can capture the dynamics of such systems more accurately. Moving to multi-component out-of-equilibrium or chemical reaction network bearing supramolecular systems, the kinetics of bond making and breaking coupled with the assembly process dictates the life-times of transient assembly. Molecular dynamics simulations with reactive force fields[77] would be a promising and hitherto unexplored approach to quantify and ultimately control the lifetime of transient assembly accurately.

The current challenges presented above will most surely be addressed with the advent of future technologies. In years to come in-situ time resolved imaging techniques may indeed pave the way to the design of next-generation supramolecular

Table 1. Table showing various features and the scope of each technique.

Techniques	Spatial Resolution	Temporal Resolution	Special Requirements/Limitations	Advantages
CLSM	~200nm	Milliseconds to Seconds	• Diffraction limited resolution	• Readily available instrument
SIM	~120nm	Seconds	-	• Fast • Standard fluorescent dyes • Super resolution imaging
STED	~50nm	Seconds	• Specific dyes needed	• Super resolution with video imaging capability
SMLM	~20nm	Seconds to Minutes	• Specific dyes needed • Redox buffer solutions	• Super resolution with best spatial resolution
LP-TEM	~1nm	Femtoseconds to Seconds	• Thin liquid sample layer • Establishing safe electron dose levels for each experiment • Sample radiation damage • Beam effects on solvent i.e., water radiolysis	• No chemical modification needed • Compatibility with elemental analysis via energy dispersive X-ray analysis EDX or EELS • Heating and electrical biasing capabilities • Chemical biasing (using electron beam to initiate chemical reactions) • Inlet/outlet flow cells to introduce chemical stimuli *in situ*
SS-AFM	~1nm	Milliseconds	• Requires stable absorption of nanostructure on solid substrate • Tip-induced mechanical damage • Loss of lateral resolution due to tip contamination	• No chemical modification needed • Video rate imaging • Possibility to introduce external solutions *in situ* • Multiparametric imaging capability, e.g., topography, mechanical property imaging
MD Simulations	Atomic to Molecular level	Nanoseconds to Milliseconds	• May not capture the actual chemistry of the system	• Molecular level insights under any experimentally relevant conditions

materials where a deep understanding of the structure and its evolution over time will drive and tailor the desired function. Moreover, the use of microfluidic channels and other flow-based liquid cells, to flow samples for imaging, will facilitate imaging of dynamic processes upon introducing external chemical stimuli and potentially optical stimuli. Most importantly, the integration of multiple techniques into a single platform will bring a paradigm shift. Thus, integrating super-resolution fluorescence imaging with a mass spectrometer and LP-TEM or SS-AFM on a single platform combined with online real-time machine learning optimization might seem fictional today but would provide us with the ultimate capability where physical, chemical and microscopic information can be obtained in real-time, in situ.

Acknowledgements

AV and MK acknowledge funding from “la Caixa” Foundation (ID 100010434) and the European Union’s Horizon 2020 research and innovation programme under the Marie Skłodowska-Curie grant agreement No 847648. The fellowship code is “LCF/BQ/PI21/11830035. MK also thanks Proyectos de Generación de Conocimiento 2021 grant from the Spanish ministry of science and innovation (PID2021-126244NA-I00). CK acknowledges support from IIT Bombay seed grant. AC acknowledges the Foundation "Bartolo Longo III Millennio" and the Institute of Nanoscience and Nanotechnology of UB (IN2UB) under the project Ajut a la Recerca Transversal (ART 2020) for financial support.

Keywords: Supramolecular Chemistry • Nanostructures • Super-resolution microscopy • Systems Chemistry • Liquid TEM

[1] T. Aida, E. W. Meijer, S. I. Stupp, *Science* **2012**, *335*, 813-817.
[2] a) C. Donau, F. Späth, M. Sosson, B. A. Kriebisch, F. Schnitter, M. Tena-Solsona, H.-S. Kang, E. Salibi, M. Sattler, H. Mutschler, *Nat. Commun.* **2020**, *11*, 5167; b) R. Chen, S. Neri, L. J. Prins, *Nat. Nanotechnol.* **2020**, *15*, 868-874; c) J. Boekhoven, W. E. Hendriksen, G. J. Koper, R. Eelkema, J. H. van Esch, *Science* **2015**, *349*, 1075-1079; d) M. Kumar, N. L. Ing, V. Narang, N. K. Wijerathne, A. I. Hochbaum, R. V. Ulijn, *Nat. Chem.* **2018**, *10*, 696-703.
[3] a) K. Das, L. Gabrielli, L. J. Prins, *Angew. Chem. Int. Ed.* **2021**, *60*, 20120-20143; b) F. Sheehan, D. Sementa, A. Jain, M. Kumar, M. Tayarani-Najjaran, D. Kroiss, R. V. Ulijn, *Chem. Rev.* **2021**, *121*, 13869-13914; c) S. De, R. Klajn, *Adv. Mater.* **2018**, *30*, 1706750; d) G. Ashkenasy, T. M. Hermans, S. Otto, A. F. Taylor, *Chem. Soc. Rev.* **2017**, *46*, 2543-2554; e) S. A. van Rossum, M. Tena-Solsona, J. H. van Esch, R. Eelkema, J. Boekhoven, *Chem. Soc. Rev.* **2017**, *46*, 5519-5535; f) A. Jain, A. Calò, D. Barceló, M. Kumar, *Anal. Bioanal. Chem* **2022**, 5105-5119; g) A. Chatterjee, A. Reja, S. Pal, D. Das, *Chem. Soc. Rev.* **2022**, *51*, 3047-3070.
[4] T. A. Klar, S. Jakobs, M. Dyba, A. Egner, S. W. Hell, *Proc. Natl. Acad. Sci. U. S. A.* **2000**, *97*, 8206-8210.
[5] J. Huff, *Nat. Methods* **2015**, *12*, i-ii.
[6] R. Kubota, K. Nagao, W. Tanaka, R. Matsumura, T. Aoyama, K. Urayama, I. Hamachi, *Nat. Commun.* **2020**, *11*, 4100.
[7] D. Axelrod, *Traffic* **2001**, *2*, 764-774.
[8] M. Samperi, B. Bdiri, C. D. Sleet, R. Markus, A. R. Mallia, L. Perez-Garcia, D. B. Amabilino, *Nat. Chem.* **2021**, *13*, 1200-1206.
[9] a) A. Colom, E. Derivery, S. Soleimanpour, C. Tomba, M. D. Molin, N. Sakai, M. Gonzalez-Gaitan, S. Matile, A. Roux, *Nat. Chem.* **2018**, *10*, 1118-1125; M. Dal Molin, Q. Veerolet, A. Colom, R. Letrun, E. Derivery, M. gonzalez-Gaitan, E, Vauthey, A. Roux, N. Sakai, S. Matile. *J. Am. Chem. Soc.* **2015**, *137*, 568-571.
[10] a) S. Pujals, L. Albertazzi, *ACS Nano* **2019**, *13*, 9707-9712; b) S. Pujals, N. Feiner-Gracia, P. Delcanale, I. Voets, L. Albertazzi, *Nat. Rev. Chem.* **2019**, *3*, 68-84.
[11] E. Betzig, G. H. Patterson, R. Sougrat, O. W. Lindwasser, S. Olenych, J. S. Bonifacino, M. W. Davidson, J. Lippincott-Schwartz, H. F. Hess, *Science* **2006**, *313*, 1642-1645.
[12] L. Albertazzi, D. van der Zwaag, C. M. Leenders, R. Fitzner, R. W. van der Hofstad, E. W. Meijer, *Science* **2014**, *344*, 491-495.
[13] M. B. Baker, L. Albertazzi, I. K. Voets, C. M. Leenders, A. R. Palmans, G. M. Pavan, E. W. Meijer, *Nat. Commun.* **2015**, *6*, 6234.
[14] R. M. da Silva, D. van der Zwaag, L. Albertazzi, S. S. Lee, E. W. Meijer, S. I. Stupp, *Nat. Commun.* **2016**, *7*, 11561.
[15] S. Pujals, K. Tao, A. Terradellas, E. Gazit, L. Albertazzi, *Chem. Commun.* **2017**, *53*, 7294-7297.
[16] J. Garcia-Calvo, J. Maillard, I. Fureraj, K. Strakova, A. Colom, V. Mercier, A. Roux, E. Vauthey, N. Sakai, A. Furstenberg, S. Matile, *J. Am. Chem. Soc.* **2020**, *142*, 12034-12038.
[17] H. Wang, Z. Feng, B. Xu, *Chem. Soc. Rev.* **2017**, *46*, 2421-2436.
[18] Q. Yao, C. Wang, M. Fu, L. Dai, J. Li, Y. Gao, *ACS Nano* **2020**, *14*, 4882-4889.
[19] R. Heintzmann, T. Huser, *Chem. Rev.* **2017**, *117*, 13890-13908.
[20] a) A. Sarkar, R. Sasmal, A. Das, A. Venugopal, S. S. Agasti, S. J. George, *Angew. Chem. Int. Ed.* **2021**, *133*, 18357-18364; b) A. Sarkar, R. Sasmal, C. Empereur-Mot, D. Bochicchio, S. V. K. Kompella, K. Sharma, S. Dhiman, B. Sundaram, S. S. Agasti, G. M. Pavan, S. J. George, *J. Am. Chem. Soc.* **2020**, *142*, 7606-7617.
[21] D. Gupta, R. Sasmal, A. Singh, J. P. Joseph, C. Miglani, S. S. Agasti, A. Pal, *Nanoscale* **2020**, *12*, 18692-18700.
[22] a) Y. M. Sigal, R. Zhou, X. J. S. Zhuang, *Science* **2018**, *361*, 880-887; b) Y. Wu, H. Shroff, *Nat. Methods* **2018**, *15*, 1011-1019.
[23] S. W. Hell, J. Wichmann, *Opt. Lett.* **1994**, *19*, 780-782.
[24] S. Onogi, H. Shigemitsu, T. Yoshii, T. Tanida, M. Ikeda, R. Kubota, I. Hamachi, *Nat. Chem.* **2016**, *8*, 743-752.
[25] a) M. Kumar, J. Son, R. H. Huang, D. Sementa, M. Lee, S. O'Brien, R. V. Ulijn, *ACS Nano* **2020**, *14*, 15056-15063; b) M. Kumar, D. Sementa, V. Narang, E. Riedo, R. V. Ulijn, *Chem. Eur. J.* **2020**, *26*, 8372-8376.
[26] A. Vinckier, I. Heyvaert, A. D'Hoore, T. McKittrick, C. Van Haesendonck, Y. Engelborghs, L. Hellemans, *Ultramicroscopy* **1995**, *57*, 337-343.
[27] K. Aratsu, R. Takeya, B. R. Pauw, M. J. Hollamby, Y. Kitamoto, N. Shimizu, H. Takagi, R. Haruki, S. I. Adachi, S. Yagai, *Nat. Commun.* **2020**, *11*, 1623.
[28] a) J. Chen, E. Zhu, J. Liu, S. Zhang, Z. Lin, X. Duan, H. Heinz, Y. Huang, J. J. De Yoreo, *Science* **2018**, *362*, 1135-1139; b) T. Fukui, T. Uchihashi, N. Sasaki, H. Watanabe, M. Takeuchi, K. Sugiyasu, *Angew. Chem. Int. Ed.* **2018**, *57*, 15465-15470; c) S. Maity, J. Ottele, G. M. Santiago, P. Frederix, P. Kroon, O. Markovitch, M. C. A. Stuart, S. J. Marrink, S. Otto, W. H. Roos, *J. Am. Chem. Soc.* **2020**, *142*, 13709-13717.
[29] O. Shyshov, S. V. Haridas, L. Pesce, H. Qi, A. Gardin, D. Bochicchio, U. Kaiser, G. M. Pavan, M. von Delius, *Nat. Commun.* **2021**, *12*, 3134.
[30] P. R. Heenan, T. T. Perkins, *ACS Nano* **2019**, *13*, 4220-4229.
[31] A. Podesta, L. Imperadori, W. Colnaghi, L. Finzi, P. Milani, D. Dunlap, *J. Microsc.* **2004**, *215*, 236-240.
[32] Z. Lv, S. Banerjee, K. Zagorski, Y. L. Lyubchenko, in *Nanoscale Imaging*, Springer, **2018**, pp. 129-143.
[33] H. Jin, F. Jiao, M. D. Daily, Y. Chen, F. Yan, Y. H. Ding, X. Zhang, E. J. Robertson, M. D. Baer, C. L. Chen, *Nat. Commun.* **2016**, *7*, 12252.
[34] N. Ashwanikumar, J. S. Plaut, B. Mostofian, S. Patel, P. Kwak, C. Sun, K. McPhail, D. M. Zuckerman, S. C. Esener, G. Sahay, *J. Control. Release* **2018**, *282*, 76-89.
[35] a) T. Ando, T. Uchihashi, N. Kodera, *Annu. Rev. Biophys.* **2013**, *42*, 393-414; b) T. Uchihashi, S. Scheuring, *Biochim. Biophys. Acta. Gen. Subj.* **2018**, *1862*, 229-240.
[36] A. Laisne, M. Ewald, T. Ando, E. Lesniewska, D. Pompon, *Bioconjugate Chem.* **2011**, *22*, 1824-1834.
[37] E. Abbe, *Archiv für mikroskopische Anatomie* **1873**, *9*, 413-468.
[38] J. Dubochet, J. Lepault, R. Freeman, J. Berriman, J. C. Homo, *J. Microsc.* **1982**, *128*, 219-237.
[39] a) J. Frank, *J. Struct. Biol.* **2017**, *200*, 303-306; b) R. Henderson, *Angew. Chem. Int. Ed.* **2018**, *57*, 10804-10825.
[40] a) N. De Jonge, F. M. Ross, *Nat. Nanotechnol.* **2011**, *6*, 695-704; b) H. Wu, H. Friedrich, J. P. Patterson, N. A. Sommerdijk, N. de Jonge, *Adv. Mater.* **2020**, *32*, 2001582; c) G. Marchello, C. De Pace, A. Duro‐Castano, G. Battaglia, L. Ruiz‐Pérez, *J. Microsc.* **2020**, *279*, 242-248.
[41] J. M. Yuk, J. Park, P. Ercius, K. Kim, D. J. Hellebusch, M. F. Crommie, J. Y. Lee, A. Zettl, A. P. Alivisatos, *Science* **2012**, *336*, 61-64.
[42] G. McMullan, S. Chen, R. Henderson, A. Faruqi, *Ultramicroscopy* **2009**, *109*, 1126-1143.
[43] J. Shui, C. Chen, L. Grabstanowicz, D. Zhao, D.-J. Liu, *Proc. Natl. Acad. Sci. U. S. A.* **2015**, *112*, 10629-10634.
[44] J. P. Patterson, P. Abellan, M. S. Denny Jr, C. Park, N. D. Browning, S. M. Cohen, J. E. Evans, N. C. Gianneschi, *J. Am. Chem. Soc.* **2015**, *137*, 7322-7328.
[45] K. M. Vailonis, K. Gnanasekaran, X. B. Powers, N. C. Gianneschi, D. M. Jenkins, *J. Am. Chem. Soc.* **2019**, *141*, 10177-10182.

[46] L. R. Parent, E. Bakalis, A. Ramírez-Hernández, J. K. Kammeyer, C. Park, J. De Pablo, F. Zerbetto, J. P. Patterson, N. C. Gianneschi, *J. Am. Chem. Soc.* **2017**, *139*, 17140-17151.
[47] A. Duro-Castano, L. Rodríguez-Arco, L. Ruiz-Pérez, C. De Pace, G. Marchello, C. Noble-Jesus, G. Battaglia, *Biomacromolecules* **2021**, *22*, 5052-5064.
[48] N. M. Schneider, M. M. Norton, B. J. Mendel, J. M. Grogan, F. M. Ross, H. H. Bau, *J. Phys. Chem. C* **2014**, *118*, 22373-22382.
[49] K. Gnanasekaran, J. Korpanty, O. Berger, N. Hampu, M. Halperin-Sternfeld, D. Cohen-Gerassi, L. Adler-Abramovich, N. C. Gianneschi, *ACS Nano* **2021**, *15*, 16542-16551.
[50] M. A. Vratsanos, N. C. Gianneschi, *ACS Nano* **2022**, *16*, 7783-7793.
[51] a) P. W. Frederix, I. Patmanidis, S. J. Marrink, *Chem. Soc. Rev.* **2018**, *47*, 3470-3489; b) A. Manandhar, M. Kang, K. Chakraborty, P. K. Tang, S. M. Loverde, *Org. Biomol. Chem.* **2017**, *15*, 7993-8005; c) O.-S. Lee, S. I. Stupp, G. C. Schatz, *J. Am. Chem. Soc.* **2011**, *133*, 3677-3683.
[52] a) M. P. Hendricks, K. Sato, L. C. Palmer, S. I. Stupp, *Acc. Chem. Res.* **2017**, *50*, 2440-2448; b) E. Moulin, J. J. Armao IV, N. Giuseppone, *Acc. Chem. Res.* **2019**, *52*, 975-983.
[53] a) S. Cantekin, T. F. de Greef, A. R. Palmans, *Chem. Soc. Rev.* **2012**, *41*, 6125-6137; b) B. N. Thota, X. Lou, D. Bochicchio, T. F. Paffen, R. P. Lafleur, J. L. van Dongen, S. Ehrmann, R. Haag, G. M. Pavan, A. R. Palmans, *Angew. Chem. Int. Ed.* **2018**, *130*, 6959-6963; c) N. M. Matsumoto, R. P. Lafleur, X. Lou, K.-C. Shih, S. P. Wijnands, C. m. Guibert, J. W. van Rosendaal, I. K. Voets, A. R. Palmans, Y. Lin, *J. Am. Chem. Soc.* **2018**, *140*, 13308-13316; d) C. Kulkarni, E. Meijer, A. R. Palmans, *Acc. Chem. Res.* **2017**, *50*, 1928-1936.
[54] a) D. B. Korlepara, S. Balasubramanian, *RSC Adv.* **2018**, *8*, 22659-22669; b) D. Bochicchio, G. M. Pavan, *Adv. Phys. X* **2018**, *3*, 1436408.
[55] a) K. K. Bejagam, G. Fiorin, M. L. Klein, S. Balasubramanian, *J. Phys. Chem. B* **2014**, *118*, 5218-5228; b) K. K. Bejagam, S. Balasubramanian, *J. Phys. Chem. B* **2015**, *119*, 5738-5746.
[56] D. Bochicchio, M. Salvalaglio, G. M. Pavan, *Nat. Commun.* **2017**, *8*, 147.
[57] A. Barducci, G. Bussi, M. Parrinello, *Phys. Rev. Lett.* **2008**, *100*, 020603.
[58] E. Krieg, M. M. Bastings, P. Besenius, B. Rybtchinski, *Chem. Rev.* **2016**, *116*, 2414-2477.
[59] C. M. Leenders, L. Albertazzi, T. Mes, M. M. Koenigs, A. R. Palmans, E. Meijer, *Chem. Commun.* **2013**, *49*, 1963-1965.
[60] D. Bochicchio, G. M. Pavan, *ACS Nano* **2017**, *11*, 1000-1011.
[61] A. L. de Marco, D. Bochicchio, A. Gardin, G. Doni, G. M. Pavan, *ACS Nano* **2021**, *15*, 14229-14241.
[62] a) Y. Wu, X. Han, Y. Su, M. Glidewell, J. S. Daniels, J. Liu, T. Sengupta, I. Rey-Suarez, R. Fischer, A. Patel, C. Combs, J. Sun, X. Wu, R. Christensen, C. Smith, L. Bao, Y. Sun, L. H. Duncan, J. Chen, Y. Pommier, Y. B. Shi, E. Murphy, S. Roy, A. Upadhyaya, D. Colon-Ramos, P. La Riviere, H. Shroff, *Nature* **2021**, *600*, 279-284; b) Y. Wu, X. Han, Y. Su, M. Glidewell, J. S. Daniels, J. Liu, T. Sengupta, I. Rey-Suarez, R. Fischer, A. Patel, C. Combs, J. Sun, X. Wu, R. Christensen, C. Smith, L. Bao, Y. Sun, L. H. Duncan, J. Chen, Y. Pommier, Y.-B. Shi, E. Murphy, S. Roy, A. Upadhyaya, D. Colón-Ramos, P. La Riviere, H. Shroff, *bioRxiv* **2021**, preprint DOI:10.1101/2021.1105.1121.445200.
[63] R. W. Taylor, V. Sandoghdar, *Nano Lett.* **2019**, *19*, 4827-4835.
[64] M. A. Lebedeva, E. Palmieri, P. Kukura, S. P. Fletcher, *ACS Nano* **2020**, *14*, 11160-11168.
[65] G. Young, N. Hundt, D. Cole, A. Fineberg, J. Andrecka, A. Tyler, A. Olerinyova, A. Ansari, E. G. Marklund, M. P. Collier, *Science* **2018**, *360*, 423-427.
[66] M. G. Howlett, A. H. Engwerda, R. J. Scanes, S. P. Fletcher, *Nat. Chem.* **2022**, *14*, 805-810.
[67] W. Guo, J. Yin, Z. Xu, W. Li, Z. Peng, C. Weststrate, X. Yu, Y. He, Z. Cao, X. Wen, *Science* **2022**, *375*, 1188-1191.
[68] G. Zhan, Z.-F. Cai, K. Strutyński, L. Yu, N. Herrmann, M. Martínez-Abadía, M. Melle-Franco, A. Mateo-Alonso, S. D. Feyter, *Nature* **2022**, *603*, 835-840.
[69] A. Dols-Perez, G. Gramse, A. Calò, G. Gomila, L. Fumagalli, *Nanoscale* **2015**, *7*, 18327-18336.
[70] R. García, R. Magerle, R. Perez, *Nat. Mater.* **2007**, *6*, 405-411.
[71] a) R. Garcia, *Chem. Soc. Rev.* **2020**, *49*, 5850-5884; b) A. Calò, A. Eleta-Lopez, P. Stoliar, D. De Sancho, S. Santos, A. Verdaguer, A. M. Bittner, *Sci. Rep.* **2016**, *6*, 21899; c) Z. Al-Rekabi, S. Contera, *Proc. Natl. Acad. Sci. U. S. A.* **2018**, *115*, 2658-2663.
[72] a) D. Alsteens, D. J. Muller, Y. F. Dufrene, *Acc. Chem. Res.* **2017**, *50*, 924-931; b) A. Calò, Y. Romin, R. Srouji, C. P. Zambirinis, N. Fan, A. Santella, E. Feng, S. Fujisawa, M. Turkekul, S. Huang, *Sci. Rep.* **2020**, *10*, 15664.
[73] a) T. Touzalin, A. L. Dauphin, S. Joiret, I. T. Lucas, E. Maisonhaute, *PCCP* **2016**, *18*, 15510-15513; b) J. Mathurin, A. Deniset-Besseau, D. Bazin, E. Dartois, M. Wagner, A. Dazzi, *J. Appl. Phys.* **2022**, *131*, 010901.
[74] a) S. Handschuh-Wang, T. Wang, X. Zhou, *RSC Adv.* **2017**, *7*, 47464-47499; b) L. Zhou, M. Cai, T. Tong, H. Wang, *Sensors* **2017**, *17*, 938; c) M. A. Beuwer, M. F. Knopper, L. Albertazzi, D. van der Zwaag, W. G. Ellenbroek, E. W. Meijer, M. W. J. Prins, P. Zijlstra, *Polym. Chem.* **2016**, *7*, 7260-7268.
[75] J. M. Voss, O. F. Harder, P. K. Olshin, M. Drabbels, U. J. Lorenz, *Chem. Phys. Lett.* **2021**, *778*, 138812.
[76] O. T. Unke, S. Chmiela, H. E. Sauceda, M. Gastegger, I. Poltavsky, K. T. Schütt, A. Tkatchenko, K.-R. Müller, *Chem. Rev.* **2021**, *121*, 10142-10186.
[77] K. Chenoweth, A. C. Van Duin, W. A. Goddard, *J. Phys. Chem. A* **2008**, *112*, 1040-1053.

10.1002/anie.202208681

WILEY-VCH

REVIEW

Entry for the Table of Contents

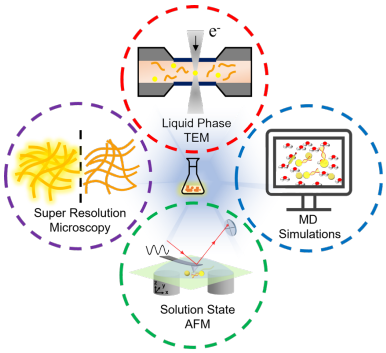

Visualizing Dynamic Nanostructures

As supramolecular chemistry begins to develop dynamic nanostructures that change over time, it becomes imperative to visualize self-assembly processes in solution in real-time. Our Review demonstrates how solution-based visualization techniques, namely optical super-resolution microscopy, atomic force and electron microscopy in liquid, and molecular dynamics simulations, have enriched our understanding of nanomaterials to obtain novel functions.

Institute and/or researcher Twitter usernames: @Mohit_Chemist, @IBECBarcelona